A

Project Report

On

Stability Study of Important Metal Organic Frameworks (MOFs) and a Review on their Gas Adsorption Properties

Submitted by

Vinay Kumar Agarwal

(Roll No: 108CH008)

In partial fulfillment of the requirements for the degree in

Bachelor of Technology in Chemical Engineering

Under the guidance of

Dr. Pradip Chowdhury

Department of Chemical Engineering

National Institute of Technology Rourkela

May, 2012

CERTIFICATE

This is certified that the work contained in the thesis entitled ***"Stability Study of Important Metal Organic Frameworks (MOFs) and a Review on their Gas Adsorption Properties,"*** *submitted by* ***Vinay Kumar Agarwal (108CH008)****, has been carried out under my supervision and this work has not been submitted elsewhere for a degree.*

Date:

Place:

(Thesis Supervisor)

Dr. Pradip Chowdhury
Assistant Professor, Department of Chemical Engineering
NIT Rourkela

Acknowledgements

First and the foremost, I would like to offer my sincere gratitude to my thesis supervisor, **Dr. Pradip Chowdhury** for his immense interest and enthusiasm on the project. His technical prowess and vast knowledge on diverse fields left quite an impression on me. He was always accessible and worked for hours with me. Although the journey was beset with complexities but I always found his helping hand. He has been a constant source of inspiration for me.

I am also thankful to all faculties and support staff of Department of Chemical Engineering, National Institute of Technology Rourkela, for their constant help and extending the departmental facilities for carrying out my project work.

I would like to extend my sincere thanks to my friends and colleagues. Last but not the least, I wish to profoundly acknowledge my parents for their constant support.

_____

(Vinay Kumar Agarwal)

108CH008

ABSTRACT

Metal Organic Frameworks (or, MOFs) have shown tremendous potential in adsorptive separation applications and gas storage owing to some of their extraordinary features in terms of specific surface area, pore volume, low to moderate heat of adsorption and fairly uniform pore size distribution. But, the success or failure of any adsorbent material largely depends on their stability in varying experimental conditions. In this work, we have highlighted the synthesis of 3 most versatile MOFs reported till date *viz*. Cu-BTC (or, HKUST-1), Cr-BDC (or, MIL-101) and Zn-BDC (or, MOF-5). Each of these MOFs after their successful synthesis and characterization were exposed to a regulated environmental condition to study the effect of moisture sensitivity. Such a study is particularly important since any real time experiment with MOF is bound to come to terms with varying degree of moisture or water vapor, especially when exposed for longer duration. After detailed experimentation we concluded that a controlled exposure to ambient conditions didn't have a severe effect on MOF's thermal stability. Cr-BDC was found to be taking up more moisture during the course of time as compared to Cu-BTC and Zn-BDC. The degree of crystallinity appeared to be reduced over the time interval and surface morphology too gets affected.

Moreover, we have carried out a comprehensive review of 3 very important industrially and environmentally important gases *viz*. H_2, CO and CO_2 on these three MOF matrices. The reason behind choosing theses gases stems out from the fact that H_2 is projected as a future fuel which may very well replace the conventional fossil fuels, both CO_2 and CO are the most important green house gases and their emission needs to be effectively arrested, mixture of these gases are emitted from various sources e.g. steam reforming of naphtha, partial oxidation of hydrocarbons, metallurgical plants etc. Apart from these facts, physical properties of each of them are quite different. H_2 is a non-polar gas whereas CO has a permanent dipole moment and CO_2 has a quadrupole moment. Studying the effects of these physical properties could be interesting from a fundamental point of view to understand the adsorption phenomenon. The retrieved experimental data from literature was model fit using standard isotherm models *viz*. Langmuir, Freundlich, Freundlich-Langmuir, Dual Site Langmuir (DSL) and Virial models. Additionally, a comparative

study between simulation data (available in literature) and experimental data (at same conditions) was carried out for a proper validation. CO was selected on the basis of its polarity and CH_4 was chosen since it is non-polar. The adsorbent for the study was Cu-BTC.

Our findings are summarized as:

(I) All the isotherm models are not equally efficient in predicting the adsorption behavior in low and high pressure regime. Freundlich-Langmuir model is seen to be the best in explaining the adsorption behavior irrespective of the type of probe or adsorbent surface.

(II) The experimental H_2 adsorption data as reported by various researchers varied considerably from lab to lab and H_2 adsorption on none of the adsorbents studied in this work satisfies the Department of Energy (DoE) target of 6.5 wt%.

(III) Cr-BDC (or, MIL-101) showed the highest affinity for CO_2. This uptake of CO_2 is the highest reported till date.

(IV) Although experimental data on CO adsorption on any MOF material is scarce, but still within our review, we have found Cr-BDC to have the highest loading of CO. The higher loading can be attributed to very high surface area (*ca*. 3000 m^2 g^{-1}) for Cr-BDC amongst the studied MOFs.

(V) The comparison of simulation with experimental data of CO and CH_4 on Cu-BTC has shown that for polar molecule e.g. CO, simulation data under predicts the experimental data whereas in the higher loading region simulation data over predicts. This is less marked for non-polar gas like CH_4. It is worth mentioning that even though there are variations in simulation result predictions with experimental data but still Grand Canonical Monte Carlo (GCMC) simulation is a strong method in predicting experimental excess adsorption data particularly when total pore volume information and single crystal XRD data is available.

CONTENTS

PAGE NO.

LIST OF TABLES

LIST OF TABLES (APPENDIX)

LIST OF FIGURES

LIST OF FIGURES

LIST OF SYMBOLS

a	Specific area of adsorbent per mole of adsorbate, $m^2\ mol^{-1}$
b	Second virial coefficient in adsorbed phase, $mmol^{-1}\ g$
b_i	Affinity Parameters
b_i^0	Affinity at reference at T_o
c	Third virial coefficient in adsorbed phase, $mmol^{-2}\ g^2$
Δh_{ads}	Enthalpy of adsorption, $kJ\ mol^{-1}$
$\Delta h_{ads,0}$	Enthalpy of adsorption at zero loading, $kJ\ mol^{-1}$
K	constants for a given adsorbate and adsorbent at T
m	Mass of solid adsorbent, g
M_t	Observed mass in gravimetric experiment, g
$M_{t,0}$	True adsorbent mass with the bucket measured in vacuum
M_{ex}	Excess amount adsorbed, g
M_w	Molecular weight of the gas
n	constants for a given adsorbate and adsorbent at a T
N	Excess amount adsorbed, $mmol\ g^{-1}$
N_i^{max}	saturation capacity
P	Pressure, bar
R	Universal gas constant, $8.314\ J\ mol^{-1}\ K^{-1}$
T	Temperature, K
T_o	reference temperature
x_i	Adsorbed phase mole fraction of species i

V_{bucket}	Bucket volume, cm^3
$V_{buoyancy}$	Buoyancy volume, cm^3
Z	Compressibility factor for the adsorbed phase

GREEK LETTERS

θ	Fractional coverage of the surface
α	Langmuir constant
ρ^{gas}	Density of gas
β	Henry constant, mmol g^{-1} bar^{-1}

CHAPTER 1

INTRODUCTION

This chapter highlights the basics on adsorption science and technology. It focuses on novel materials called metal organic frameworks (or, MOFs). The background of the present thesis work is aptly explained. The objectives are also properly highlighted.

1.1 Prelude

Separation can be defined as a process that transforms a mixture of substance into two or more product that differs from each other in composition. The process is difficult to achieve because it is opposite of mixing, a process favored by the second law of thermodynamics. Separation steps accounts for the major production cost in chemical and petrochemical industry.

The surface of solid represents a discontinuity of its structure. The forces acting at the surface is unsaturated. Hence, when the solid is exposed to a gas, the gas molecule will form bonds with it and become attached. This phenomenon is termed as ***Adsorption*****.** Adsorption is the adhesion of molecules of gas, liquid or dissolved solids to a surface. It differs from absorption in which a fluid permeates through or is dissolved by a liquid or a solid. Adsorption occurs because the atoms or ions at the surface of a solid are extremely reactive. Unlike their counterparts in the interior of the substance, they have unfulfilled valence requirements. The unused bonding capability of the surface atoms or ions may be used to bond molecules from the gas or solution phase to the surface of the solid. This process creates a film of the adsorbate (the molecules or atoms being accumulated) on the surface of the adsorbent. It differs from absorption, in which a fluid permeates or is dissolved by a liquid or solid. Forces of attraction exist between adsorbate and adsorbent and due to these forces of attraction, heat energy is released. So adsorption is an exothermic process [**1**].

1.2 Types of adsorption

Forces of attraction exist between adsorbate and adsorbent. These forces of attraction can be due to Vander Waal forces of attraction which are weak forces or due to chemical bond which are strong forces of attraction. On the basis of type of forces of attraction existing between adsorbate and adsorbent, adsorption can be classified into two types: Physical Adsorption or Chemical Adsorption [**2**].

1.2.1 Physical Adsorption or Physisorption

When the force of attraction existing between adsorbate and adsorbent are weak Vander Waal forces of attraction, the process is called physical adsorption or ***Physisorption***. Physical Adsorption takes place with formation of multilayer of adsorbate on adsorbent. It has low enthalpy of adsorption i.e. $\mathbf{\Delta H}_{\mathbf{ads}}$=20~40 kJ mol^{-1}.

1.2.2 Chemical Adsorption or Chemisorption

When the force of attraction existing between adsorbate and adsorbent are chemical forces of attraction or chemical bond, the process is called chemical adsorption or ***chemisorption***. Chemisorption takes place with formation of unilayer of adsorbate on adsorbent. It has high enthalpy of adsorption i.e. $\mathbf{\Delta H}_{\mathbf{ads}}$= 200~400 kJ mol^{-1}.

1.3 Novel Adsorbents

New materials usher new technologies. Synthesizing novel materials is always reflected as a corner stone in technological developments. Until recently, zeolites and activated carbons are thought to be the indispensable in adsorption based unit operations. But as the need grows for more efficient, economical and highly specific functions, conventional adsorbents were found ill equipped to handle such problems. Although, improved synthesis and different post-treatment procedures of zeolites and activated carbon resulted into some of their derivatives but the need of the hour was to design and synthesize materials that could be more effective.

In the quest for designing novel adsorbents, attention has been paid to develop hybrid structures involving both inorganic and organic components by employing novel synthetic routes. The general concept was to take advantage of both the metal coordination and functionalities of the organic components. The concept of reticular synthesis which can be described as the process of assembling judiciously designed rigid molecular building blocks into predetermined ordered structures or networks, held together by strong bonding is found to be the key to the true design of novel solid-state materials. Researchers have envisioned that to fully realize the benefits of designing crystalline solid state frameworks the structural integrity and rigidity of the molecular building blocks must remain unaltered throughout the construction process: key feature of reticular synthesis [**3**]. The said mechanism plays a pivotal role in producing robust porous materials by connecting rigid rod-like organic moieties with inflexible inorganic clusters acting as joints. The length and functionalities of the organic units determine the size and chemical environment of the resulting void spaces. Accordingly, the concept of 'tailor-made' materials finally realized. Appropriate selection of starting materials can give rise to myriad of different structures. Within a short period of time a large variety of extended structures have been successfully prepared and the collection of compounds has been given various names e.g. 'co-ordination polymers', 'hybrid organic-inorganic materials', 'organic zeolite analogues' or 'metal organic frameworks'. Although each terminology signifies certain aspects of the materials it encompasses but for a solid to be truly called a 'Metal Organic Framework' or MOF, it must possess robustness implying strong bonding, assembling units are available for modification by organic synthesis and geometrically a well-defined structure [**4**].

1.4 Background of present research work

Some conventional well-known adsorbents include: silica gel, activated alumina, activated carbon, carbon molecular sieves and zeolites. Each of these adsorbents has certain specific features that have been exploited over the years in various industrially challenging applications ranging from adsorptive gas separation/purification, ion-exchange and catalysis. In this present context, the term 'Novel' signifies a new class of hybrid adsorbents popularly known as 'metal organic frameworks' or MOFs and 'covalent organic frameworks' or COFs.

Metal organic frameworks are relatively new class of crystalline porous material consists of metal cluster connected by organic ligands. They are crystalline compound consisting of metal ions/cluster coordinated to often rigid organic molecules to form one, two, three dimensional structures that can be porous. The pore size and surface properties of these materials can be tuned to a great extent with relative ease by choosing appropriate metal centers and organic ligands. This structural flexibility generated interest in these materials for the application ranging from gas storage and separation, catalysis and so forth. The main advantages of MOFs are: Good crystallinity akin to zeolites, high porosity and structural and functional diversity.

The experimental data of gas adsorption on MOFs vary from lab to lab. Especially with H_2, the excess amount adsorbed reported by various research groups on similar surfaces varied considerably both at cryogenic conditions as well as at room temperature. Similar observations are also made for CO and CO_2. Additionally, it is worth mentioning that each of these gases is quite different from one another on fundamental aspects. H_2 is a non-polar gas whereas CO_2 possess high quadrupole moment and CO has a permanent dipole. Owing to their differences in electrical properties, interactions of these gases with various adsorbent surfaces would be highly interesting and attempts have been made by various research groups.

1.4.1 Selection of MOF

A careful review of the literature reveals more than 2,000 different MOF structures being synthesized and characterized. Although the number speaks volumes about their variation in structural configuration but not all are stable. Thermal and chemical stability, along with high surface area is what researchers look for in a good adsorbent to be effective at the industrial level. Cu-BTC (or HKUST-1), Cr-BDC (or MIL-101) and Zn-BDC (or, MOF-5) frameworks

possess all the desirable qualities that set them apart from others. Not only they have very high specific surface areas but also show better stability. Some of their characteristic features include:

- High specific surface area (~1000 to 5000 m^2/g), large pore volume (~0.7-2.5 cc/g) and light weight or low packing density
- Low to moderate heat of adsorption (15-20 kJ/mol)
- Good thermal and chemical stability

1.4.2 Selection of Gases

A brief illustration on each of them is highlighted below:

[A] **Hydrogen**: At present, carbon based fossil fuels provide ~ 80% of the world's energy demands and they are the main source of the increasing level of CO_2 in the atmosphere, responsible for serious climate change. H_2 being the clean and green fuel is gaining rapid popularity as an alternate source of energy. The development of a safe and efficient hydrogen storage system is urgently needed for the realization of hydrogen as a future fuel.

[B] **Carbon dioxide and Carbon monoxide**: Apart from being harmful greenhouse gases, the mixtures of CO/CO_2 are found in a variety of industrial off gases e.g. coming out of metallurgical plants, in synthesis gas (from steam reforming), partial oxidation of many hydrocarbons and coal. The capture and removal of these gases is important to meet environmental regulations and adsorption can be a viable option.

1.5 Research Objectives

The main objectives of our research can be classified in the following categories:

[**A**] As top-down approach it is of paramount importance to have a knowledge about the details of material synthesis and post-synthesis treatments for synthesizing a more stable and immune MOF structure. In this work, we aimed at synthesizing 3 most versatile MOF structures *viz*. Cu-BTC, Cr-BDC and Zn-BDC. Each of them would be exposed to a controlled ambient conditions (with fairly constant relative humidity) to examine their immunity and thermal stability. Such a study is particularly important since any real time experiment with MOF is bound to come to

terms with varying degree of moisture or water vapor, especially when exposed for longer duration and hence the affect requires to be verified.

[**B**] A comprehensive literature review is done to make a database on adsorption of H_2, CO and CO_2 on various adsorbents with special emphasis on MOFs. Consistency is maintained in selecting the scale and units used for an ease in comparison. Judicious interpolation and extrapolation is done wherever required for finding accurate experimental data. Such a study is very useful and handy in getting ready-made updated information on progress made in the experimental front with these probe molecules.

[**C**] The experimental data extracted from various literatures (using "windig" software) will be tried to fit with standard isotherm models e.g. Langmuir, Freundlich, Freundlich-Langmuir, Dual Site Langmuir (DSL) and Virial models.

[**D**] Being geometrically symmetrical and regular, plenty of research has been initiated on the simulation of adsorption of various probes on many MOF surfaces. Grand Canonical Monte Carlo simulation popularly known as GCMC is one such technique. Although, GCMC simulations are known for their fair prediction and accuracy but still it requires to be validated by comparing with authentic experimental data. In our present work, we aimed at comparing the experimental data with simulation results under similar conditions for a better understanding and validation.

CHAPTER 2

LITERATURE REVIEW

In this chapter a brief review on metal organic frameworks (MOFs) is given. A general overview on adsorption of H_2, CO and CO_2 on various conventional and novel adsorbent materials is also represented in tabular form. The intention is to highlight the frequency of work in this field and gradual improvement in experimental data on adsorption of these gases on MOFs and other conventionally known adsorbents *viz*. zeolites, activated carbon etc.

2.1 Metal Organic Frameworks (MOFs)

2.1.1 Brief Review

"Metal Organic Frameworks" or MOFs represent a class of novel materials that has caught the attention of researchers owing to their great diversity in structures resulting from co-ordination between inorganic metal atoms/ions and organic ligands as linkers. Proper selection of metal atoms/ions and organic linkers leads to innumerable possibilities in the co-ordination geometry with wide variation in structural architecture. A few very attractive motifs include honeycomb, brickwall, bilayer, ladder, herringbone, diamondoid, rectangular grid, and octahedral geometries. Metal Organic Frameworks (MOFs) which forms as a result of combination of an inorganic metal atom/ion as a node with an organic ligand as a linker can be classified to be a relatively new group of materials. Ever since initial reports on its synthesis, there has been a spurt in research activities owing to some of their characteristic features. The most important features include: extremely high specific surface area (*ca*. 800-5000 m^2 g^{-1}) and large pore volume (*ca*. 0.8-2.5 cc g^{-1}), uniform pore size distribution and tunable or tailor-made pores.

2.1.2 MOF Architecture

The key to successfully designing metal organic frameworks lies in the use of linkers meant to achieve desired network topologies by connecting transition-metal centers or polynuclear clusters serving as nodes of the network. Myriad of different possibilities are there depending on our choice of metal atoms/ions and organic linkers. Flexibility or the rigidity of the frameworks is greatly affected by the choice of organic linker in the structure. To illustrate the complete behavior let us consider the following example [**3**]

In Figure 2.1 (**A**), we have the assembly of a tetrahedrally coordinated metal center and a linear organic linker like 4, 4´-bipyridine. It results in a structure with an expanded diamond topology. Each bond of the diamond network is replaced by a sequence of bonds that expands the networks and yields void space proportional to the length of the linker. In Figure 2.1 (**B**) the organic linker is 1, 4-benzene dicarboxylate. It allows for the formation of an aggregate of metal ions into M-O-C clusters that generally referred as secondary building units (SBUs) which finally extends into a cube.

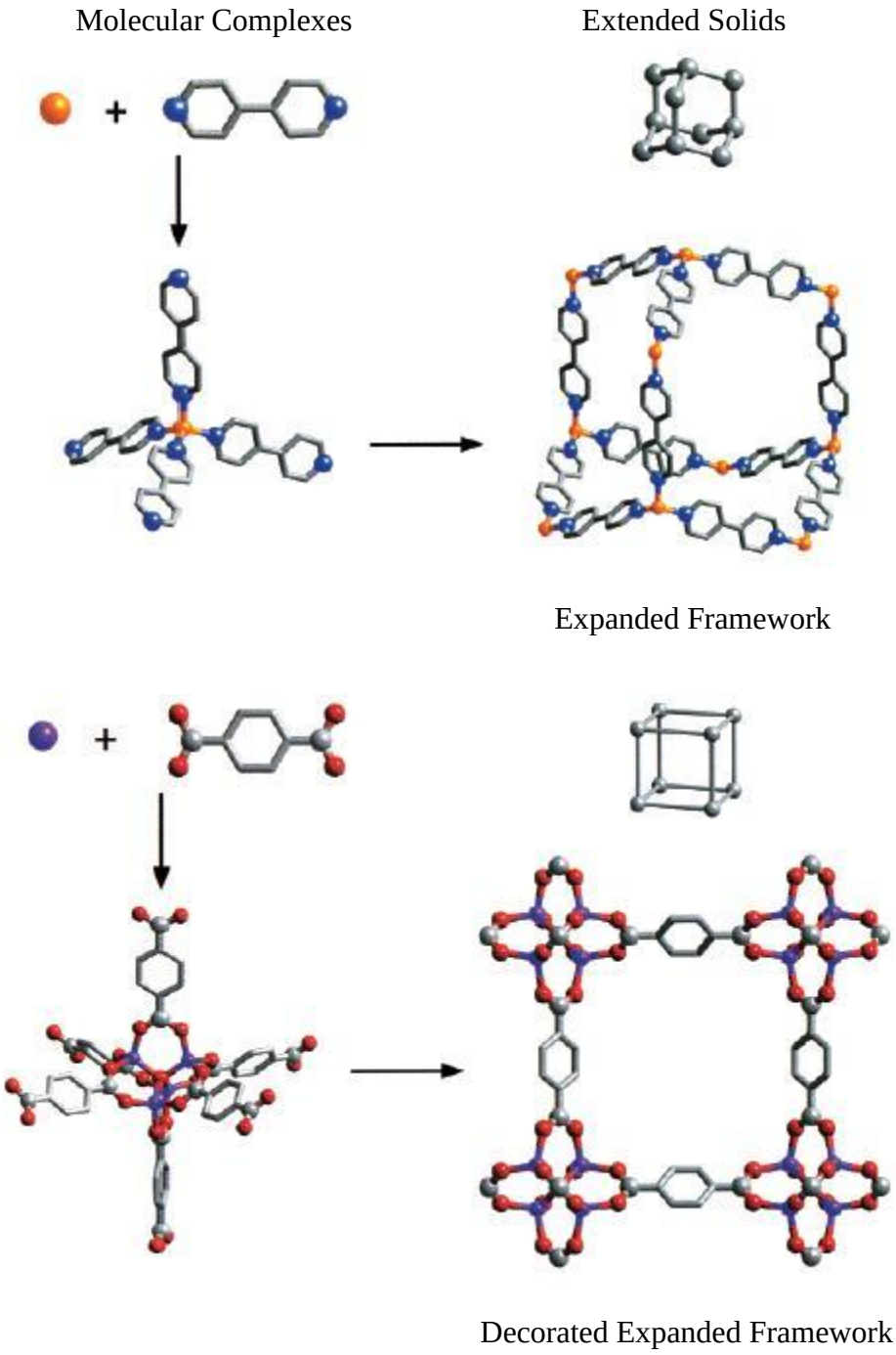

Figure 2.1: Assembly of Metal Organic Frameworks. (**A**) Flexible metal-bipyridine structures with expanded diamond topology (Metal-orange, Carbon-gray, Nitrogen-blue) (**B**) Rigid metal-carboxylate clusters expanding into a cube (Metal-purple, Carbon-gray, Oxygen-red). For the sake of clarity all hydrogen atoms are not shown [**3**].

2.1.3 Salient Features of MOFs

Some of the characteristic features of MOFs include:

(a) High surface area (*ca*. 800-5000 $m^2 g^{-1}$) and pore volume (*ca*. 0.5-2.5 ml g^{-1})

(b) Highly crystalline and can be synthesized in pure form with less crystal imperfections

(c) Uniform pore size distribution akin to zeolites and hence good molecular sieving properties

(d) Low to moderate heat of adsorption and hence can act as a good gas storage medium

(e) Low bulk packing density i.e. lighter in weight

Although MOFs have shown some remarkable features but still there are certain unresolved issues which hindered its application at the industrial level. Most importantly, the thermal and chemical stability of MOFs is a bottleneck which requires to be overcome. Out of an excess of 2000 MOF matrix synthesized and analyzed, very few could withstand a temperature in excess of 300^oC. The frameworks collapse and showed low robustness at moderate to high temperatures. Moreover, frameworks also showed less immunity under aqueous and various organic mediums. Qualitatively as well as quantitatively speaking, same MOF synthesized at same conditions (keeping constant stoichiometry) following same recipes at times tend to yield products with varying percentage purities. Since, percentage yields and product purities of different batches vary; care must be taken during synthesis and post-synthesis treatments. It is also observed that MOFs undergoing adsorption mechanism in pressure swing adsorption (PSA) column undergo physical deformation after a few cycles or swings. The effect of high pressure is also a cause of concern before they can be approved to be industrially more viable.

2.1.4 Important MOFs

A careful review of literature shows that out of an excess of more than 2000 variants of MOFs reported till date: the Zn, Cu and Cr based MOFs have found a niche in the scientific community. The most widely studied MOF series since its inception can be grouped as follows:

(I) The Isoreticular Metal Organic Frameworks or IRMOF series (MOF-5 being also known as IRMOF-1).

(II) Cu-BTC or HKUST-1

(III) MatérialInstitut Lavoisier or MIL series

The improvement in their surface areas and pore volume as reported by various researchers over the years is summarized in a tabular form.

Table 2.1: The surface area and pore volume data of Cu-BTC, Cr-BDC and Zn-BDC (as reported by various research groups in literature)

MOF	Synthesis Method	Surface Area (m^2/g)	Pore Volume (cm^3/g)	References
Cu-BTC	Hydrothermal	1482	0.828	**[5]**
	Hydrothermal	698	0.39	
	_	1635	0.82	
	_	1504	_	
	Hydrothermal	692	0.333	**[6]**
	Hydrothermal	964,1333 (different batch)	0.658	**[7]**
	Hydrothermal	_	0.37	**[8]**
	Hydrothermal	_	0.41	**[9]**
	Hydrothermal	1781	_	**[10]**
	Hydrothermal	1507	0.75	**[11]**
	Hydrothermal	_	0.32	**[12]**

MOF	Synthesis Method	Surface Area (m^2/g)	Pore Volume (cm^3/g)	References
Cr-BDC (MIL-101)	Hydrothermal	3197	1.73	**[13]**
		3148	1.53	
		2250	1.24	
		2800	1.37	**[14]**
		3780	1.74	
		4230	2.15	
		2931	1.45	**[15]**
		2220	1.13	**[16]**

MOF	Synthesis Method	BET (m^2/g)	Pore Volume (cm^3/g)	References
Zn-BDC (MOF-5)	Solvothermal	_	0.61-0.54	**[17]**
		666	0.21	
		650	0.2	**[18]**
		3362	_	**[19]**
		572	0.28	**[20]**
		2296	_	**[21]**

2.2 The Adsorptive Gases or Probe Molecules

For the present study three gases are chosen. The reasoning and logic behind selecting them are already given in chapter-1.

An illustrative literature review is being carried out on adsorption of these gases on various types of adsorbents including novel MOFs. We think such a study is significant to create a small database for important information.

Table 2.2: Literature Review of Experimental Data on Adsorption of H_2 on various MOFs (as reported over the years)

Researcher	**Material**	**Work done (Theoretical/ Experimental)**	**Ref**
Rosi et al.	MOF-5	Adsorbed H_2 up to 4.5 wt% at 78 K and 1% at room temperature and pressure of 20 bar.	[22]
Rowsell et al.	IRMOF-1,8,11,18 & MOF-177	All the measurements were carried out at 77 K and up to atmospheric pressure and H_2 uptake were found to be 13.2, 15.0, 16.2, 8.9 and 12.5 mg g^{-1} respectively.	[23]
Wong-Foy et al.	IRMOF-1,6,11,20 MOF-177,74 HKUST-1	The measurements were carried out at 77 K and pressure up to 90 bar and the saturation capacity varied widely for each MOF.	[24]
Pan et al.	MMOM	Adsorbed up to 1wt% at room temperature and pressure approximately 48 atmosphere.	[25]
Férey et al.	MIL-53	3.2 wt% (Cr^{3+} based) and 3.8 wt% (Al^{3+} based) at 77 K and pressure under 1.6 MPa.	[26]
Latroche et al.	MIL-100, 101	At room temperature capacity was 0.15 wt% with pressure below 7.33 MPa, but at 77 K it goes up to 3.28 wt% at pressure below 2.65 MPa (for MIL-100) whereas for MIL-101 the capacity was as high as 6.1 wt% at 77 K.	[27]

Table 2.3: Literature Review of Experimental Data on Adsorption of CO_2 on various adsorbents including MOFs (as reported over the years)

Adsorbent	Pressure	Temperature	Loading	Isosteric Heat	$-\Delta h_{ads,0}$ (kJ mol^{-1})	Henry constant / β (mmol g^{-1} bar^{-1})	Ref
	P / (bar)	T / K	N / mmol g^{-1}	$-\Delta h_{ads}$ / (kJ mol^{-1})			
13X	4, 12	298	6.0, 7.0				[28]
5A	1.2, 5.2, 10	303	3.07, 3.5, 3.6	19.64			[29]
AC (Norit R1)	0.99, 4.97, 49.9	298	2.23, 5.65, 10			4.74	[30]
AC (Norit)	38	313	0.24				[31]
MIL-53 (Al)	5, 10, 25	304	3.3, 8.2, 10.4	35-17			[10]
MIL-53 (Cr)	5, 10, 25	304	3.3, 8.0, 10	35-17			[10]
Cu-BTC	4, 12	298	10, 12.5				[28]
	0.97	313	1.6		14.5		[32]
Cu-BTC (sample b)	0.9	295	4.7			6.24	[33]
Cu-BTC (sample c)	10, 17.5	298	7.4, 8.0				[33]
H-Mordenite	1.01, 1.39	303	2.2, 2.38				[34]
H-ZSM-5	1.03	296.9	1.9	38-27	38		[35]
IRMOF-1		300			14.5		[32]
	0.8	298	0.57				[36]
IRMOF-3	1.03	313	1.25		19.5		[32]
	1	298	0.91				[36]
MIL-100	10, 60	303	9, 18.5	63-20	62		[37]
MIL-101[a]	10, 34	303	9, 25	32-18			[37]

Adsorbent	Pressure	Temperature	Loading	Isosteric Heat	$-\Delta h_{ads,0}$ (kJ mol^{-1})	Henry constant / β (mmol g^{-1} bar^{-1})	Ref
	P / (bar)	T / K	N / mmol g^{-1}	$-\Delta h_{ads}$ / (kJ mol^{-1})			
MIL-101 (sample b)	10, 60	303	12, 32	32-18			[37]
MIL-101 (sample c)	10, 40	303	14.5, 34.8	45-25	44		[37]
MIL-47	5, 10, 20	304	6.3, 8.8, 11.4	25-20			[10]
	1	298	1.59				[36]
MOF-177	1	298	0.68				[36]
MOF-5	1.01	296	2.1				[38]
NaETS-4	1.07	288	3.26	67			[39]
NaX	0.29	304.4	4.6	49-36	49.1		[35]
	0.69	305.8	5.4				[35]
	1.19	312	4.64	50-31			[40]
	1	293	6	47-35	47		[41]
		293.15			48		[42]
Na-ZSM-5	0.72	297.1	1.9	50-29	50		[39]
Silicalite	0.79, 8.63, 17	304.4	1.31, 2.8, 3	24.065		3.85	[43]
	1.04, 5.17, 20.4	307.8	1.45, 2.5, 3	28			[44]
	1, 4.5	313	1.45, 2.4				[45]
	0.8	303.6	1.5	27-28	27.2		[46]
ZIF-8	0.9	298	0.8				[36]

Table 2.4: Literature Review of Experimental Data on Adsorption of COon various adsorbents including MOFs (as reported over the years)

Adsorbent	Pressure	Temperature	Loading	Isosteric Heat	$-\Delta h_{ads,0}$ (kJ mol^{-1})	Henry constant / β (mmol g^{-1} bar^{-1})	Ref
	P / (bar)	T / K	N / mmol g^{-1}	$-\Delta h_{ads}$ / (kJ mol^{-1})			
5A	1.2, 5.2, 10	303	1.03, 1.81, 2.1	13.18			[29]
Cu-BTC (sample b)	1	295	0.8			1.27	[33]
Silicalite	1.18, 4.1, 7.3	305.3	0.27, 0.72, 1.0	16.656		0.26	[43]
	1.23, 4.07, 7.4	341.4	0.14, 0.41, 0.7				[43]

CHAPTER 3

THEORY ON ADSORPTION ISOTHERMS AND MEASUREMENTS

This chapter summarizes on various types of adsorption isotherms based on IUPAC nomenclature. Isotherm models are also discussed in detail. Details on adsorption measurement techniques are also discussed.

3.1 Adsorption Isotherms

Adsorption of a pure component of gas on a solid at equilibrium can be represented by the following function:

$$N = f(P,T) \qquad (3.1)$$

N is the amount adsorbed in cc STP per gm, P is the pressure and T is temperature.

At constant temperature, the amount of gas adsorbed onto a solid surface is only a function of P and is known as adsorption isotherm [**1**]. During the process of adsorption, adsorbate molecules get attached to the adsorbent surface physically due to van der Waal's forces of attraction.

$$\text{Adsorbate} + \text{Adsorbent} \underset{\text{desorption}}{\overset{\text{Adsorption}}{\rightleftharpoons}} \text{Adsorption}$$

$$A + B \rightleftharpoons AB$$

According to Le-Chatelier principle, the direction of equilibrium would shift in that direction where the stress can be relieved. In case of application of excess of pressure to the equilibrium system, the equilibrium will shift in the direction where the number of molecules decreases. Since number of molecules decreases in forward direction, with the increases in pressure, forward direction of equilibrium will be favored.

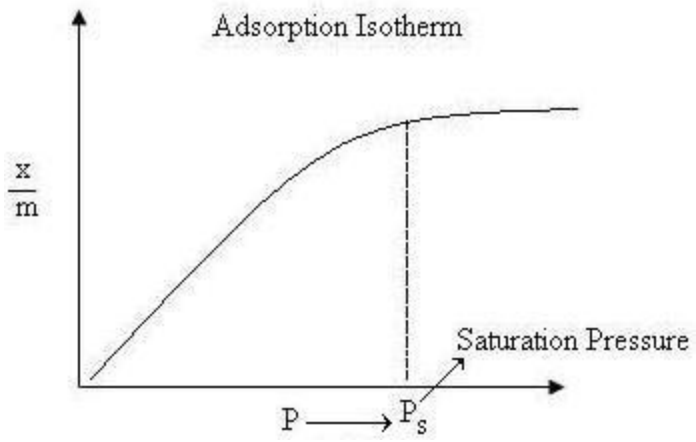

Figure 3.1: Basic Adsorption Isotherm

From the graph, we can predict that after saturation pressure Ps, adsorption does not occur anymore. This can be explained by the fact that there are limited numbers of vacancies on the surface of the adsorbent. At high pressure a stage is reached when all the sites are occupied and further increase in pressure does not cause any difference in adsorption process. At high pressure, Adsorption is independent of pressure.

3.1.1 Types of Isotherms

The great majority of isotherms observed to-date can be classified into five types as shown in figure given in next page.

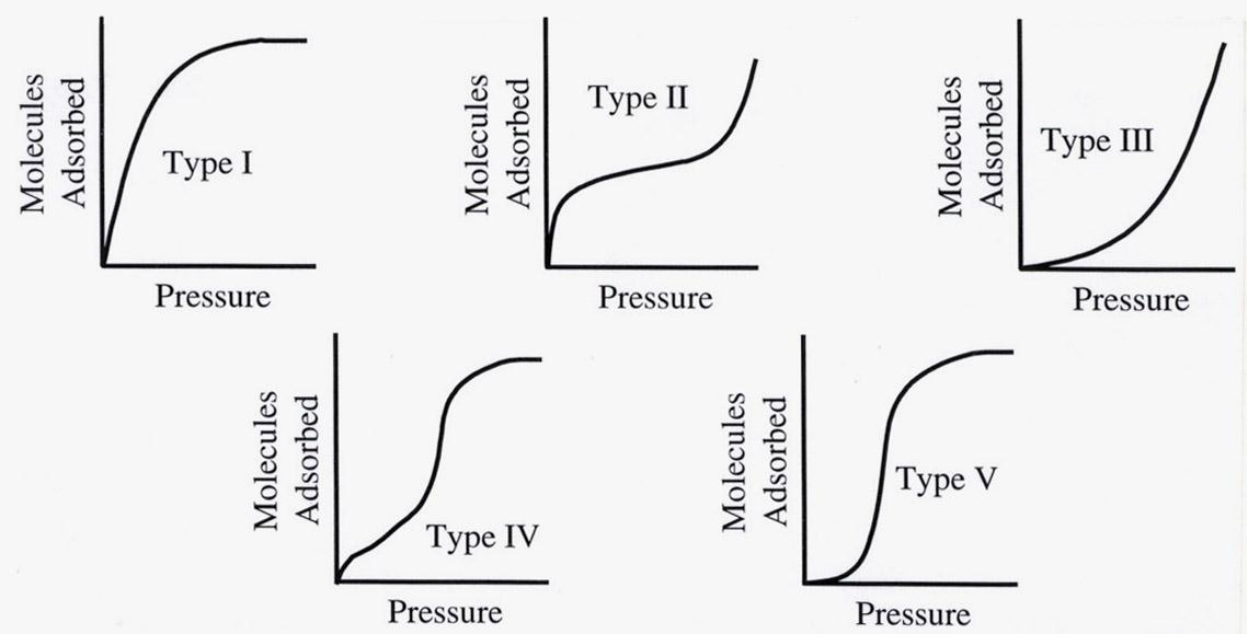

Figure 3.2: The five types of adsorption isotherms described by Brunauer [47]

Type I: This type of isotherm arises when only one type of adsorption site is present. It depicts monolayer adsorption. Initially, surface fills randomly then eventually the solid starts to saturates when surface gets up filled or pores get filled up for a porous material then the adsorption becomes constant and don't increase with increasing pressure and the pressure is termed as Saturation pressure.

Type II: This type arises when there is more than one adsorption site present on the solid. At first initial rapid adsorption takes place when first site is saturated second starts to fill up. Second site could be a second monolayer, a second site on the surface. In porous material, it can be a second type of pore.

Type III: This type arises when there are strong attractive interactions between the molecules leading to condensation. Initially, no adsorption takes place when pressure increases it leads to nucleation eventually liquids condense on the surface.

Type IV: At lower pressure region of graph is quite similar to Type II. This explains formation of monolayer followed by multilayer. The saturation level reaches at a pressure below the saturation vapor pressure .This can be explained on the basis of a possibility of gases getting

condensed in the tiny capillary pores of adsorbent at pressure below the saturation pressure of the gas.

Type V: It is a another case for attractive interaction initially no adsorption takes place later nucleation starts which leads to formation of liquid drops and coverage saturates when no more space is left to hold adsorbate.

Type I and II are the most frequently encountered in separation process. Many theories and models have been developed to interpret these types of isotherms.

3.2 Isotherm Models

Important isotherm models are discussed in this section.

3.2.1 Freundlich Adsorption Isotherm [1]

In 1909, Freundlich gave an empirical expression representing the isothermal variation of adsorption of a quantity of gas adsorbed by unit mass of solid adsorbent with pressure. This equation is known as Freundlich adsorption isotherm or Freundlich adsorption equation. The Freundlich adsorption isotherm is mathematically expressed as:

$$\frac{x}{m} = KP^{\frac{1}{n}} \tag{3.2}$$

It is also written as

$$\log(\frac{x}{m}) = \log k + (\frac{1}{n}) \log P \tag{3.3}$$

Or

$$\frac{x}{m} = Kc^{\frac{1}{n}} \tag{3.4}$$

3.2.2 Langmuir Adsorption Isotherm [48]

When Freundlich isotherm failed at higher temperature Irving Langmuir in 1916 derived a simple adsorption isotherm, on theoretical considerations based on kinetic theory of gases. This is named as Langmuir adsorption isotherm. The *Langmuir equation* relates the coverage or adsorption of molecules on a solid surface to gas pressure or concentration of a medium above the solid surface at a fixed temperature.

The equation is stated as:

$$\theta = \frac{\alpha P}{1+\alpha P} \qquad (3.5)$$

Where, θ is the fractional coverage of the surface, P is the gas pressure or concentration, α is a constant. The constant α is the *Langmuir adsorption constant*and increases with an increase in the binding energy of adsorption and with a decrease in temperature.

The following assumptions are used by Langmuir while deriving the equation:

- Adsorption occurs on a fixed number of sites.
- Each site can only take one adsorbate molecule
- All sites are energetically equivalent
- Interaction between adsorbed molecules are neglected as they are assumed to be small compared to sorbate/sorbent interactions
- Dynamic equilibrium exists between adsorbed gaseous molecules and the free gaseous molecules.

3.2.3 Freundlich-Langmuir isotherm

A combined equation of Freundlich and Langmuir was proposed in the following form:

$$q = \frac{(qm)bP^n}{1+bP^n} \tag{3.6}$$

3.2.4 Dual Site Langmuir (DSL) Isotherm [47]

The Dual Site Langmuir (DSL) model is a four-parameter isotherm, distinguishing two categories of different active sorption sites in the adsorbent, each one following a Langmuir adsorption behavior

$$N = \frac{N_1^{\max} b_1 P}{1+b_1 P} + \frac{N_2^{\max} b_2 P}{1+b_2 P} \tag{3.7}$$

Where, $N_i^{\max}$ and b_i denotes saturation capacity and affinity parameters for sites of type 'i' respectively. The temperature dependency is included through affinity parameters via

$$b_i = b_i^0 \exp\left[\frac{-\Delta h_{ads}^{(i)}}{R}\left(\frac{1}{T}-\frac{1}{T_0}\right)\right] \tag{3.8}$$

Where, b_i^0 is the affinity at reference at T_0 and $-\Delta h_{ads}^{(i)}$ is the enthalpy of adsorption on site i with respect to temperature T_0 . The Henry's constant in this case is given by

$$H = N_1^{\max} b_1 + N_2^{\max} b_2 \tag{3.9}$$

3.2.5 Virial Isotherm

Based on virial equation of state of the form

$$\frac{\pi a}{RT} = 1 + \frac{b}{a} + \frac{c}{a^2} \qquad (3.10)$$

For the two-dimensional surface phase the virial isotherm model can be derived and is represented by

$$\ln(P/N) = k + bN + cN^2 \qquad (3.11)$$

e^{-k} Is the Henry constant and is related to the gas-solid interactions only. The other higher coefficients *viz.* b , c etc. are called as second and third Virial coefficients respectively.

The temperature dependency of Virial coefficients is given by

$$k = k_0 + \frac{k_1}{T} \qquad (3.12)$$

$$b = b_0 + \frac{b_1}{T} \qquad (3.13)$$

$$c = c_0 + \frac{c_1}{T} \qquad (3.14)$$

The physical interpretations of the virial coefficients are strictly valid only for homogeneous adsorbents at low coverage. Since virial equation is open ended, there is no limit on the amount adsorbed as the pressure is increased. But, this can lead to erroneous results if the virial equation is extrapolated beyond the range of data. However, within the temperature and pressure limits of the data, virial equation is flexible and thermodynamically consistent. The virial equation is also reliable to calculate Henry's law constants with good accuracy. In fact in a virial domain plot [$\ln(P/N)$ vs N] or [$\ln(f/N)$ vs N] the intercept is k and is directly related to Henry constant. Henry's constant H is given by

$$H = e^{-k} \qquad (3.15)$$

3.2.6 Virial-Langmuir (V-L) Isotherm

The Langmuir equation usually assumes energetic homogeneous surface, rarely possible in realistic situation. On the other hand, virial equation is flexible, thermodynamically correct and describes the heterogeneity of the surface. However, the virial model does not explain the saturation at high pressure, a phenomena observed in many cases.

To overcome this limitation, virial model is modified for an additional term to introduce saturation behavior at high pressure. The regular isotherm is given by Eq. (3.11) and the modified equation known as Virial-Langmuir isotherm is given by

$$P = \frac{N}{H}\left[\frac{N^{\max}}{N^{\max} - N}\right]\exp[bN + cN^2] \qquad (N < N^{\max}) \tag{3.16}$$

Here, H is Henry constant; b , c are virial coefficients; $N^{\max}$ is the saturation capacity.

If all the virial coefficients in the Eq. (3.16) are zero, the above expression reduces to the well-known Langmuir equation.

The temperature dependency of the parameters H , b and c in this case is given by the following expressions similar to those as described in the preceding paragraph. Saturation capacity $N^{\max}$ is also expressed with similar functionality.

$$N^{\max} = \beta^{\max,0} + \frac{\beta^{\max,1}}{T} \tag{3.17}$$

3.3 Measurement of Adsorption Isotherms

3.3.1 Pure Gas Adsorption Measurements Using Gravimetry

Various methods are available to measure pure gas adsorption isotherm. The important methods include gravimetry, volumetry and gas chromatography. Gravimetry is a fast and direct measurement technique and is gaining wide spread popularity amongst experimentalists. A typical gravimetric experimental setup is shown in Figure 3.3.

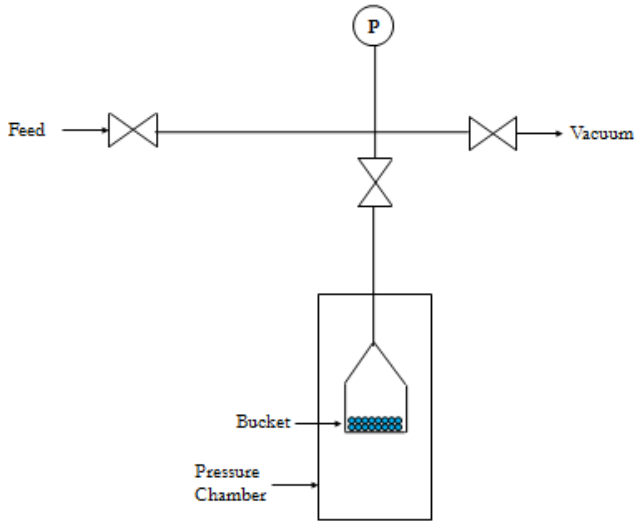

Figure 3.3: Typical gravimetric experimental setup

The adsorbent is loaded in a bucket which is on the other hand suspended from a micro balance. The sample is completely activated by keeping the pressure chamber at a high activation temperature, under vacuum. Sometimes a flow of an inert gas is utilized to facilitate flushing of desorbed components, if the system design allows for such an operation. After activation the pressure chamber is completely vacuumed, isolated and is cooled down to experimental temperature. The true adsorbent mass with the weight of the bucket, $M_{t,0}$ is measured *in vacuum*. The solid is then exposed to the gas of interest at some pressure P. At equilibrium, the observed mass M_t is related to the Gibbs' excess amount adsorbed, M_{ex} by the relation,

$$M_{ex} = M_t - M_{t,0} + V_{buoyancy}\rho^{gas} \qquad (3.18)$$

The last term on RHS accounts for the buoyancy correction on the sample and bucket. The density of the gas is usually obtained from an EoS. Some recently developed commercial balances allow simultaneous gas density measurements **[49]**.

The buoyancy volume $V_{buoyancy}$ is typically measured through Eq. (3.18) for measurements conducted using helium, with the assumption that $M_{ex} = 0$ (i.e. helium does not adsorb under experimental conditions). Once calculated from the helium experiments, $V_{buoyancy}$ is then used to calculate the Gibbs' excess amount adsorbed for all other adsorbing gases via Eq. (3.18). The buoyancy volume $V_{buoyancy}$ is the sum of the impenetrable solid volume ($V_s.m$)of an adsorbent of mass m andthe difference between the volumes of the balance assembly (buckets, hang downs etc.) between the sample and reference sides. Thus measurement of buoyancy volume fixes the Gibbs' dividing surface.

This method is the simplest in adsorption equilibrium measurements. The operator has control over the final pressure in the system. It is possible to obtain the true mass of the solid after complete desorption in vacuum. Only small amount of solid sample (often less than 1 gm) is needed. By itself this method can be used only for pure component measurements.

CHAPTER 4

EXPERIMENTAL WORKS AND DATA RETRIEVAL

This chapter illustrates MOF synthesis methods, specifically Cu-BTC, Cr-BDC and Zn-BDC. An improvised method studying the stability of the adsorbent samples at controlled ambient conditions is also elaborated. Finally, data retrieval methods are also discussed.

4.1 Synthesis of Cu-BTC

Cu-BTC or HKUST-1 was first reported by Chui et al. [50]. This method reported by Liu et al. and is a modification of previous works by Roswell and Yaghi [51]. 1, 3, 5-benzenetricarboxylic acid (1.0 g) was dissolved in 30 ml of a 1:1 mixture of ethanol/N, N-dimethylformamide (DMF). In another flask, Copper (II) Nitrate trihydrate (2.077 g) was dissolved in 15 ml water. The two solutions were then mixed and stirred for 10 min. They were then transferred into Teflon-lined stainless steel autoclave and heated at 373 K for 10 hours. The reaction vessel was cooled to room temperature normally. The resulting blue crystals were isolated by filtration and extracted with methanol overnight using a Soxhlet extractor to remove solvated DMF. The product was then dried at room temperature.

4.2 Synthesis of Cr-BDC

Cr-BDC or MIL-101 was synthesized hydrothermally following the published work of Ferey et al. [52]. The reaction was carried out in a Teflon lined stainless steel autoclave where a stoichiometric mixture of $Cr(NO_3)_3.9H_2O$, de-ionized water, 1,4-benzene dicarboxylic acid and HF was placed for 8 hrs at 493 K. Post-synthesis treatments of MIL-101 sample was crucial since significant amount of needle shaped colorless crystals of terephthalic acid (H_2BDC) formed as a by-product.

4.3 Synthesis of Zn-BDC

Zn-BDC on the other hand was synthesized following the original procedure described by Henrik Fanø Clausen et al. [53] followed by the modified route of Jinping Li et al. [54]. Zn $(NO_3)_2.6H_2O$ (6 g), and H_2BDC (1.7 g) were dissolved in DMF (20 ml). The solution was then transferred into Teflon- lined autoclave, which was heated at 373 K for 24 h. The reaction products were cooled to room temperature, and the solid obtained were collected by centrifugation, washed with DMF, and dried at room temperature.

4.4 Characterization

Characterization was performed using SEM, Powder XRD, TGA and BET surface area analysis. The membrane morphologies were observed via scanning electron microscopy (SEM, JEOL JSM-6480 LV) equipped with an energy dispersive X-ray spectrometer (EDX). Prior to imaging, each sample was platinum coated in a specialized device to increase the conductivity for a better imaging. The synthesized samples were subjected to X-ray diffraction by a diffractometer (XRD, Philips Analytical, PW-3040) equipped with the graphite monochromatizedCuKα radiation (λ=1.5406Å) in 2θ angles ranging from 5^o to 75^o with a step size of 2 degree and scanning rate 1 minute. BET surface area analysis was performed by BET surface area analyzer (Autosorb-1, Quantachrome). The relative pressure in BET surface area calculation was between 0.05-0.35. Finally, thermal analyses of samples were carried out in detail in a TGA apparatus, SHIMADZU (DTG 60 H). 60 µl alumina crucibles were used during TGA analysis.

4.5 Stability Analysis

Each of the batches of synthesized MOF samples was protected in a standard plastic vial of 25 ml volume. Each of the vials was filled up to a certain pre-determined level to set aside some empty space above the adsorbent surface. Small perforations were made in the top corners of the vial and it was kept in a controlled environment of 85~90% relative humidity for 12 weeks. Samples were re-analyzed to check for its stability subsequently.

4.6 Data Retrieval

All experimental data for our present study were retrieved from literature. 'Windig' software was used extensively for this purpose. Judicious interpolation and extrapolation was done wherever required. Model fitting was carried out using 'MATLAB' (version: 7.3.0.267). Various isotherm models were tried and tested on the experimental data to get the best fit. Model fit parameters were evaluated from model equations and the physical significance of each of the parameters was tried to be explained to understand the adsorption mechanism.

CHAPTER 5

RESULTS AND DISCUSSION

This chapter summarizes all the results. All experimental data for H_2, CO and CO_2 obtained from literature is fit with standard isotherm models and compared. Interesting observations are made and explained in detail. The effects of atmospheric condition onto synthesized MOF morphology are also explained. Comparison of experimental data with simulation data at same condition is also made and elaborated.

5.1 Comparison of Pure Gas Adsorption Isotherms of H_2, CO and CO_2

The pure component excess adsorption data retrieved from literature are either gravimetrically or volumetrically measured by various researchers across the globe. A complete summary table of our review is already shown in tables 2.2, 2.3 and 2.4 respectively. We are convinced that such a study is not only important for making a database for comparison but also give an important picture on chronological developments over the years.

Now, if we shift our attention on H_2, being projected as one of the most important future fuel, we come across many interesting observations. H_2 being a non-polar gas with very small kinetic diameter, it is always challenging to store H_2 in adsorbed mode. Conventional methods of storing H_2 in cryogenic state or compressed state proved too costly and inefficient exercise. The Department of Energy (USA) target for storing H_2 in adsorbed medium by 2010 was 6.5 wt%. Now if we focus our attention to table 2.2 we can readily see that researchers are falling way below the set target. The importance of MOFs can be gauged from the fact that they possess huge specific surface area, unparalleled by any known adsorbents till date and hence MOFs are projected as “would be” material for storing significant amount of H_2 at moderate pressure with faster kinetics. But an experienced eye can readily see the expected results and the results we have across different laboratories. The data reported in table 2.2 are mostly measured at cryogenic conditions i.e. at 77 K and moderate to high pressures. Interestingly, data reported on same MOF by two different groups vary quite significantly. The lack of consistency on measured

data with H_2 on MOFs is a cause of concern and needs to be addressed. It is also important to mention here that H_2 adsorption data measured at room temperature is way below the DoE target and this is especially important since any practical realization of adsorbed mode H_2 storage is only feasible if the amount adsorbed is significantly high at room/practical temperature. An illustrative documentation on the measured experimental data of H_2 adsorption on various novel adsorbents by different research groups is shown in ***Appendix***. A particular case study is shown in the following figure. The experimental data obtained is tried to be fit with standard isotherm models. Figures 5.1, 5.2 and 5.3 show the isotherm fits and Tables 5.1, 5.2 and 5.3 show the fit parameters.

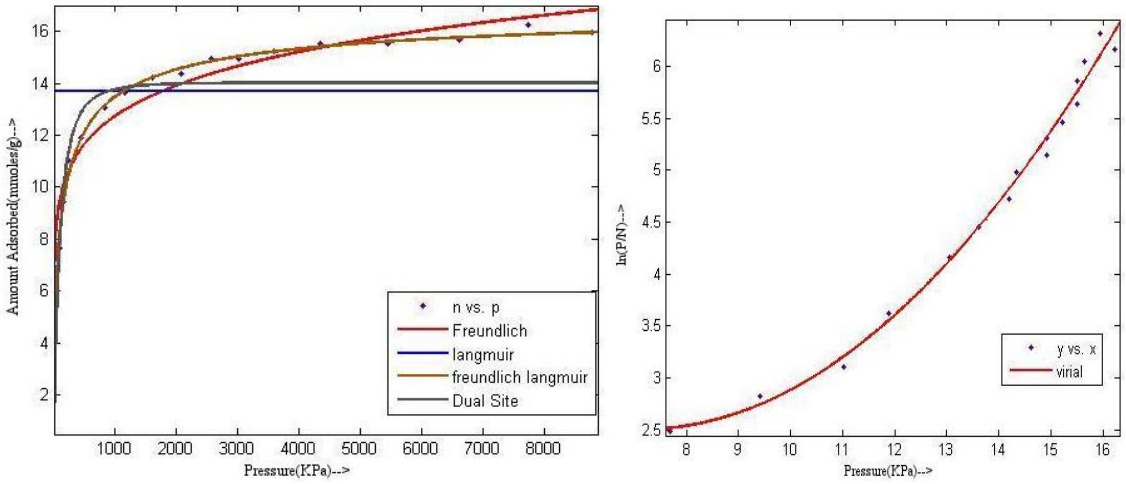

(A) (B)

Figure 5.1: Isotherm model fits of H_2 adsorption data on Cu-BTC [23] at 77 K (**A**) Conventional domain (**B**) Virial domain

Table 5.1: Model fit parameters of H_2 adsorption data on Cu-BTC at 77 K

Isotherm Model	**Fitting Parameter**	**Regression Coefficient**
Freundlich	K = 5.258 n = 0.128	0.996
Langmuir	Bad Fit	Bad Fit
Freundlich Langmuir	b_L = 0.05722 n = 0.603 q_m= 17.130	0.9934
Dual Site Langmuir	b_1 = 0.01857 b_2 = -5927 N_1^{max} = 14.02 N_2^{max} = 0.3935	0.9974
Virial	b = -0.6599 c = 0.0463 k = 4.851	0.991

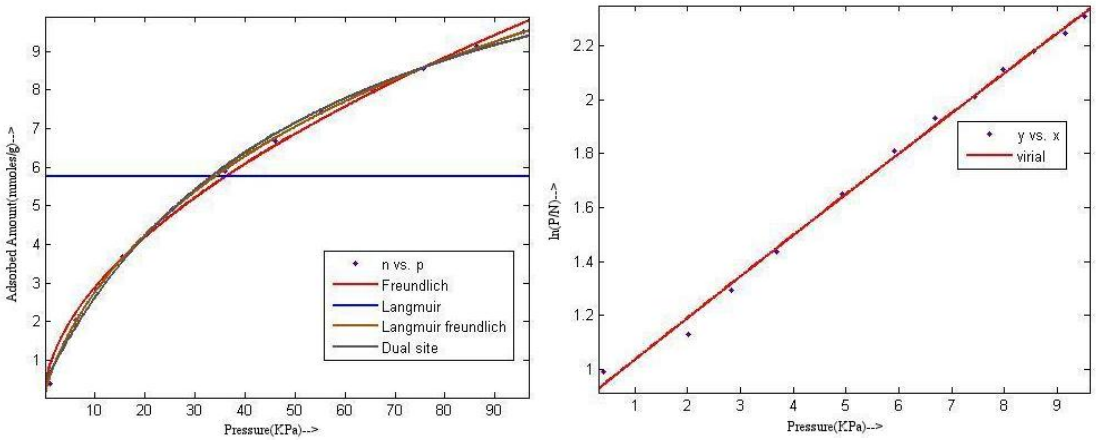

(A) (B)

Figure 5.2: Isotherm model fits of H_2 adsorption data on Cr-BDC [15] at 77 K (**A**) Conventional domain (**B**) Virial domain

Table 5.2: Model fit parameters of H_2 adsorption data on Cr-BDC at 77 K

Model	**Fitting Parameter**	**Regression Coefficient**
Freundlich	K =0.8217 n=0.5422	0.9957
Langmuir	Bad Fit	Bad Fit
Freundlich Langmuir	b_L=0.02609 n= 0.7533 q_m= 21.2	0.9995
Dual Site Langmuir	b_1 =0.01857 b_2 = -5927 N_1^{max}= 14.02 N_2^{max}= 0.3935	0.9974
Virial	b = 0.1562 c = -0.0005128 k = 0.88	0.9957

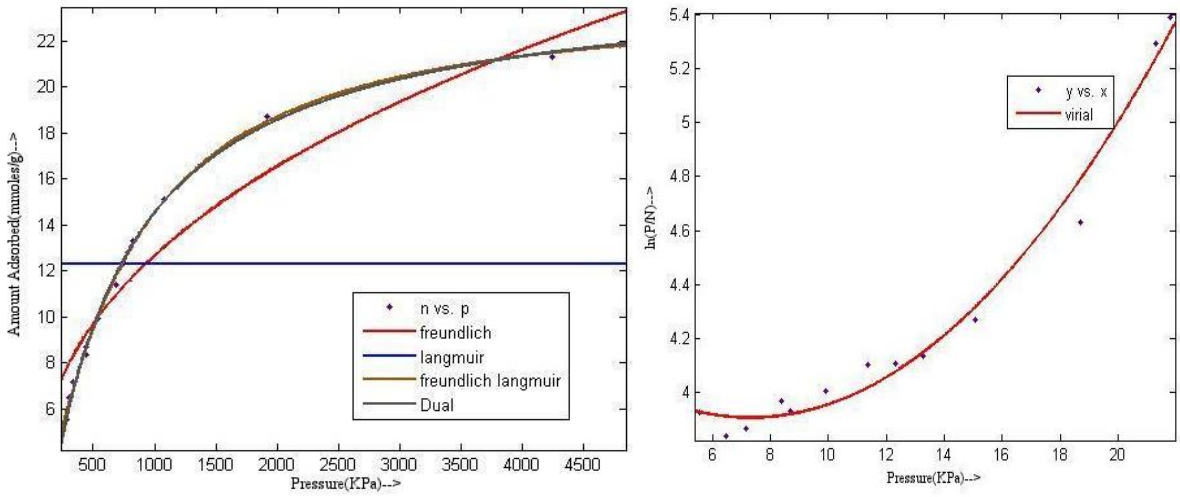

(A) (B)

Figure 5.3: Isotherm model fits of H_2 adsorption data on Zn-BDC [21] at 87 K (**A**) Conventional domain (**B**) Virial domain

Table 5.3: Model fit parameters of H_2 adsorption data on Zn-BDC at 87 K

Model	**Fitting Parameter**	**Regression Coefficient**
Freundlich	K = 0.8722 n = 0.3871	0.929
Langmuir	Bad Fit	Bad Fit
Freundlich Langmuir	b_L = 0.0002892 n = 1.244 q_m = 23.76	0.9984
Dual Site Langmuir	b_1 = -1.225 b_2 = 0.001834 N_1^{max} = -4.433 N_2^{max} = 29.27	0.9971
Virial	b = -0.09972 c = 0.00681 k = 4.269	0.9828

Tables 2.3 and 2.4 elaborate the excess adsorption data of CO_2 and CO on various types of adsorbent surfaces including novel MOFs. MOFs have shown a greater affinity for both CO and CO_2 as compared to other conventional adsorbents. Polar zeolites have performed comparatively better as compared to their non-polar counterparts, activated carbon etc. Amongst all MOFs on which CO_2 and CO gas adsorption was measured, Cr-BDC or MIL-101 has reported the highest uptake. The reason can be attributed to higher surface area for Cr-BDC (*ca*. 3000 m^2/gm) as compared to Cu-BTC (approximately 1500 m^2/gm). Although, experimental data on CO adsorption on any MOF is scarce, a few recent findings on Cr-BDC and Cu-BTC do indicate a difference in uptake. Cr-BDC showed greater affinity for CO as well compared to other adsorbents studied in this work. The experimental findings on adsorption of CO and CO_2 on important MOFs of our consideration are given in ***Appendix***. The following figures illustrate some of our model fits on experimental data (retrieved from literature) both for CO_2 and CO.

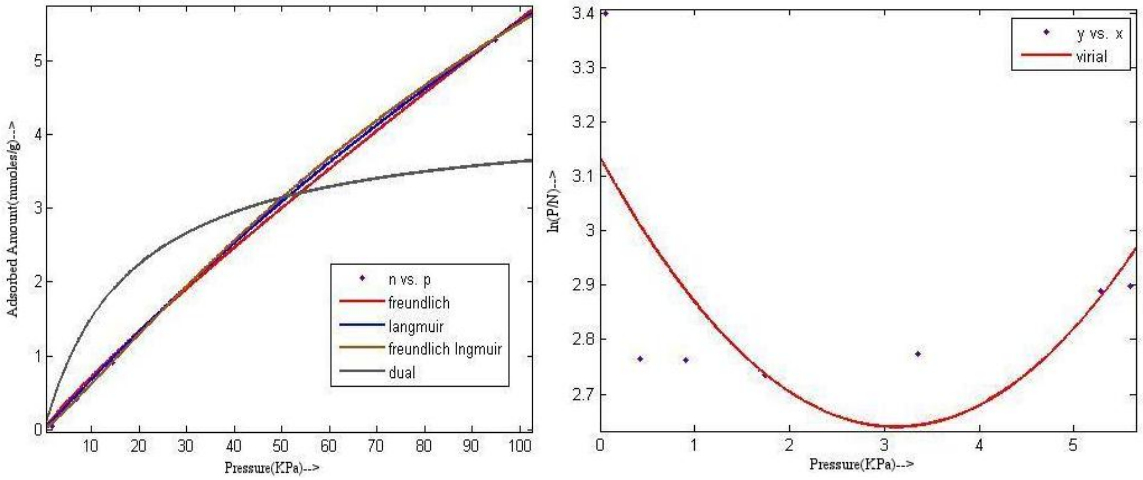

(A) (B)

Figure 5.4: Isotherm model fits of CO_2 adsorption data on Cu-BTC [58] at 293 K (**A**) Conventional domain (**B**) Virial domain

Table 5.4: Model fit parameters of CO_2adsorption data on Cu-BTC at 293 K

Model	**Fitting Parameter**	**Regression Coefficient**
Freundlich	K = 0.09316 n = 0.8878	0.9985
Langmuir	α = 0.002655 q_m= 26.34	0.9996
Freundlich Langmuir	b_L = 0.003189 n = 1.122 q_m = 15.35	0.999
Dual Site Langmuir	b_1 = 0.0518 b_2 = 0.06719 N_1^{max}= 3.475 N_2^{max}=0.8244	0.7163
Virial	b = -0.3172 c = 0.05084 k =3.135	0.4693

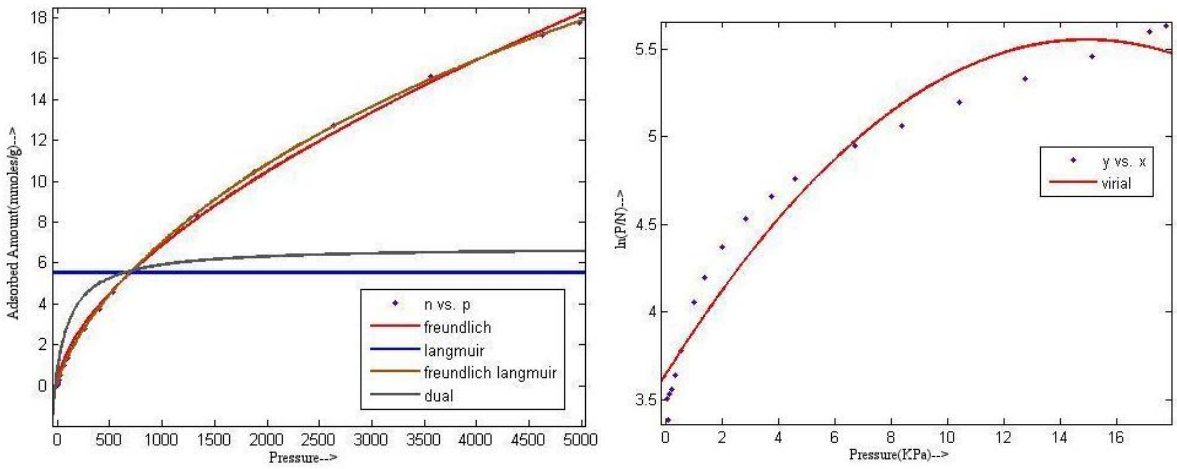

(A) (B)

Figure 5.5: Isotherm model fits of CO_2 adsorption data on Cr-BDC [55] at 318 K (**A**) Conventional domain (**B**) Virial domain

Table 5.5: Model fit parameters of CO_2 adsorption data on Cr-BDC at 318 K

Model	**Fitting Parameter**	**Regression Coefficient**
Freundlich	K = 0.1037 n = 0.6069	0.9986
Langmuir	Bad Fit	Bad Fit
Freundlich Langmuir	b_L = 0.000879 n = 0.746 q_m = 53.21	0.999
Dual Site Langmuir	b_1= 0.005957 b_2 = 26.6 N_1^{max}= 6.056 N_2^{max}= 0.7357	0.4401
Virial	b = 0.2566 c = -0.008601 k = 3.642	0.9539

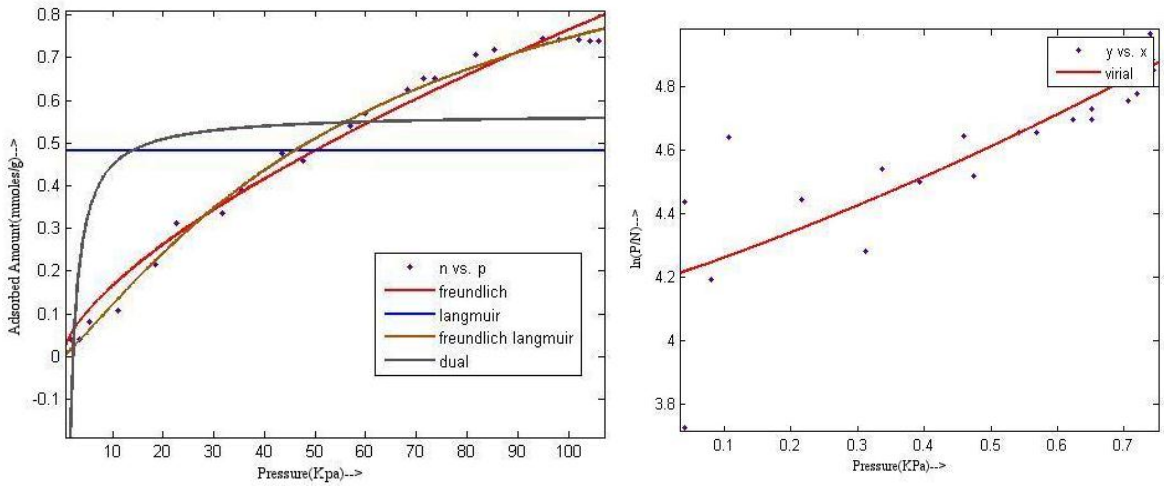

(A) (B)

Figure 5.6: Isotherm model fits of CO_2 adsorption data on Zn-BDC [59]at 298 K (**A**) Conventional domain (**B**) Virial domain

Table 5.6: Model fit parameters of CO_2 adsorption data on Zn-BDC at 298 K

Model	**Fitting Parameter**	**Regression Coefficient**
Freundlich	K = 0.03578 n = 0.6652	0.9822
Langmuir	Bad Fit	Bad Fit
Freundlich Langmuir	b_L = 0.007456 n = 1.187 q_m= 1.169	0.9935
Dual Site Langmuir	b_1 = -8.737 b_2 =-4569 N_1^{max}= -10.56 N_2^{max}=11.13	0.4747
Virial	b = 0.7078 c = 0.2751 k = 4.188	0.6947

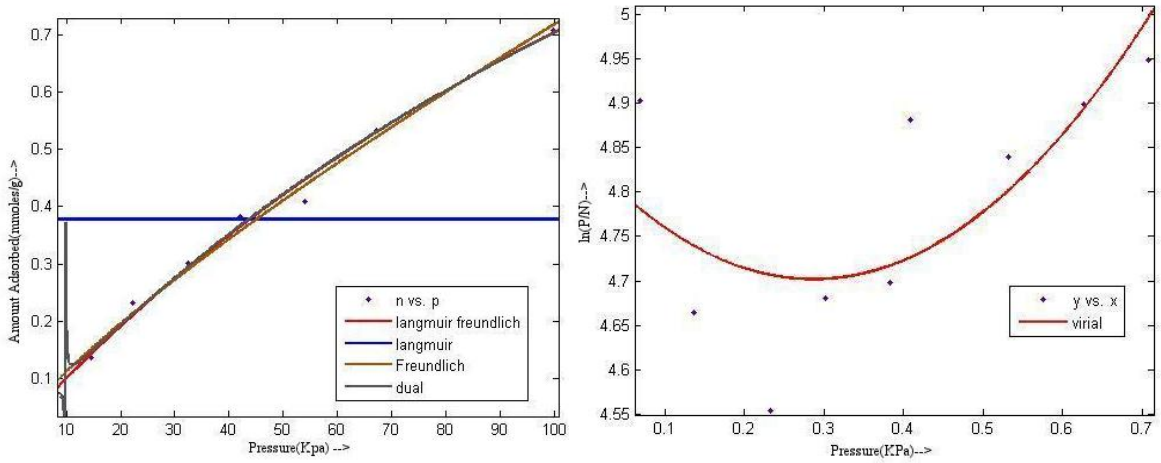

(A) (B)

Figure 5.7: Isotherm model fits of CO adsorption data on Cu-BTC [56] at 295 K (**A**) Conventional domain (**B**) Virial domain

Table 5.7: Model fit parameters of CO adsorption data on Cu-BTC at 295 K

Model	**Fitting Parameter**	**Regression Coefficient**
Freundlich	K = 0.01754 n = 0.8061	0.9902
Langmuir	Bad Fit	Bad Fit
Freundlich Langmuir	b_L = 0.004789 n = 0.9948 q_m = 2.213	0.992
Dual Site Langmuir	b_1 = 0.004922 b_2 = -0.1022 N_1^{max}=2.127 N_2^{max}=0.001582	0.9936
Virial	b = -0.9506 c =1.658 k =4.838	0.5257

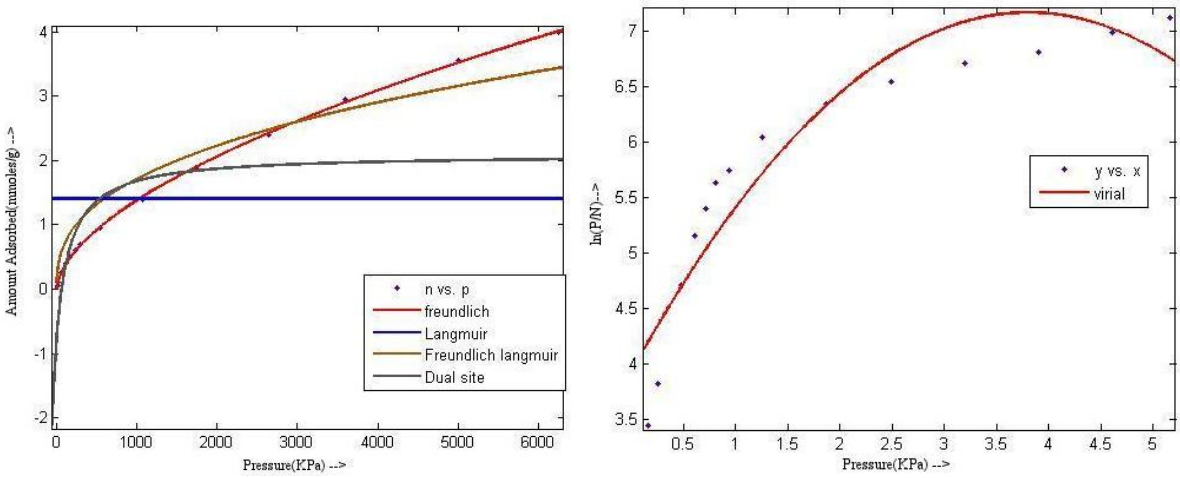

(A) (B)

Figure 5.8: Isotherm model fits of CO adsorption data on Cr-BDC [55] at 353 K (**A**) Conventional domain (**B**) Virial domain

Table 5.8: Model fit parameters of CO adsorption data on Cr-BDC at 353 K

Model	Fitting Parameter	Regression Coefficient
Freundlich	K = 0.04252 n = 0.5486	0.9981
Langmuir	Bad Fit	Bad Fit
Freundlich Langmuir	$b_L = 7.87e^{-005}$ n = 0.3492 $q_m = 2634$	0.9207
Dual Site Langmuir	$b_1 = 1923$ $b_2 = 0.0009134$ $N_1^{max} = 0.2996$ $N_2^{max} = 4.133$	0.9077
Virial	b = 1.71 c = -0.2249 k = 3.923	0.8821

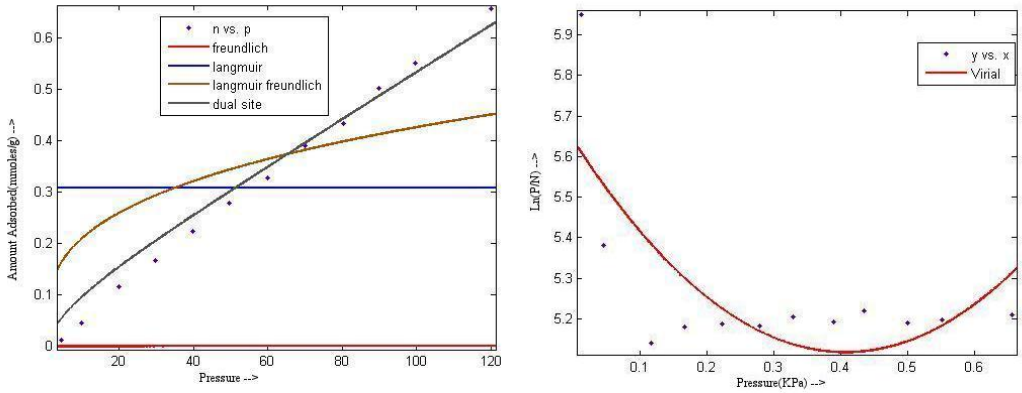

(A) (B)

Figure 5.9: Isotherm model fits of CO adsorption data on Zn-BDC [57]at 298 K (**A**) Conventional domain (**B**) Virial domain

Table 5.9: Model fit parameters of CO adsorption data on Zn-BDC at 298 K

Modal	**Fitting Parameter**	**Regression Coefficient**
Freundlich	Bad Fit	Bad Fit
Langmuir	Bad Fit	Bad Fit
Freundlich Langmuir	b_L = 0.02609 n = 0.7533 q_m = 21.2	0.9995
Dual Site Langmuir	b_1 = 0.1434 b_2 = 9.451e-006 N_1^{max} = 0.08675 N_2^{max}= 478.5	0.9974
Virial	b = -2.562 c = 3.149 k = 5.639	0.5476

5.2 Comparison of Experimental [55] Data with Simulation [56] Data

It is a popular and logical practice in the research community to establish the adsorption loading on various adsorbents using effective computational methods. Grand Canonical Mote Carlo (GCMC) simulation is widely regarded method. Not only simulation methods are fast and less cumbersome as compared to the experimental techniques but also they give fairly accurate results for geometrically uniform crystals. Although acceptance of any simulation data is subject to validation using experimentally obtained data. Since MOFs are known for their geometrical uniformity (having uniform pore size distribution) it is quite obvious to run GCMC simulation on them provided we know the total pore volume. The adsorption result that we get using simulation is the absolute adsorption as opposed to excess adsorption for experimentally measured data. In the following figure GCMC data of CO adsorption on Cu-BTC with experimental data measured at similar conditions is compared. Many interesting observations are made based on the comparison.

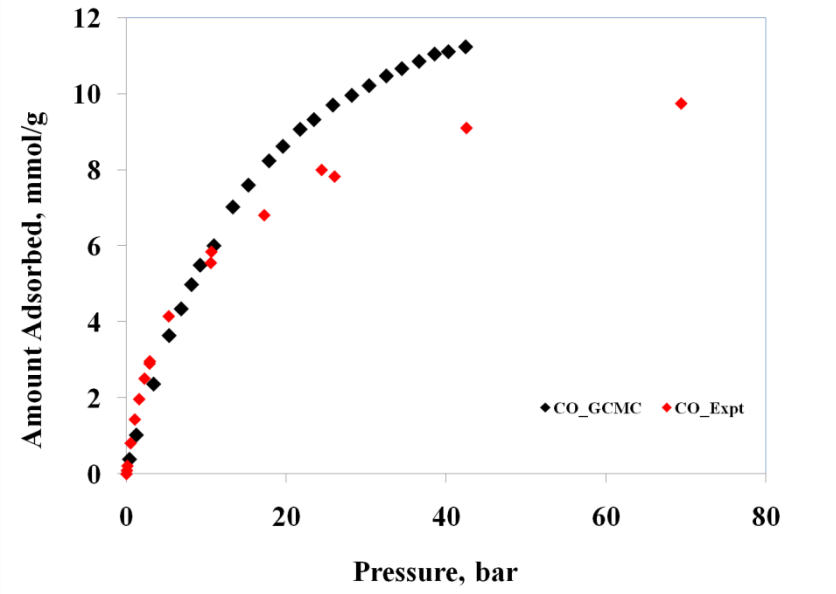

Figure 5.10: Comparison of GCMC simulation data [56] with experimental data [55] of CO adsorption on Cu-BTC

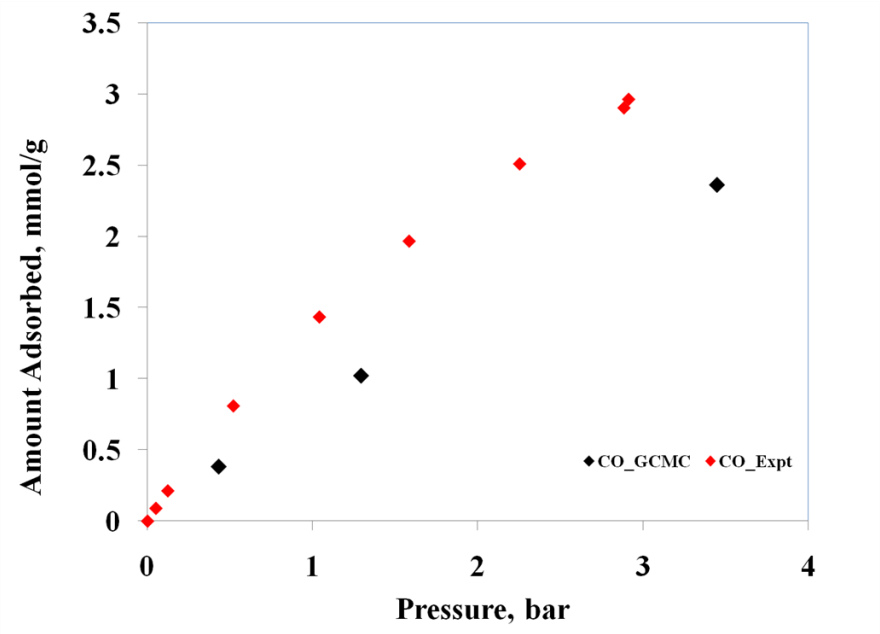

Figure 5.11: Comparison of GCMC simulation data [56] with experimental data [55] of CO adsorption on Cu-BTC at low pressure regime

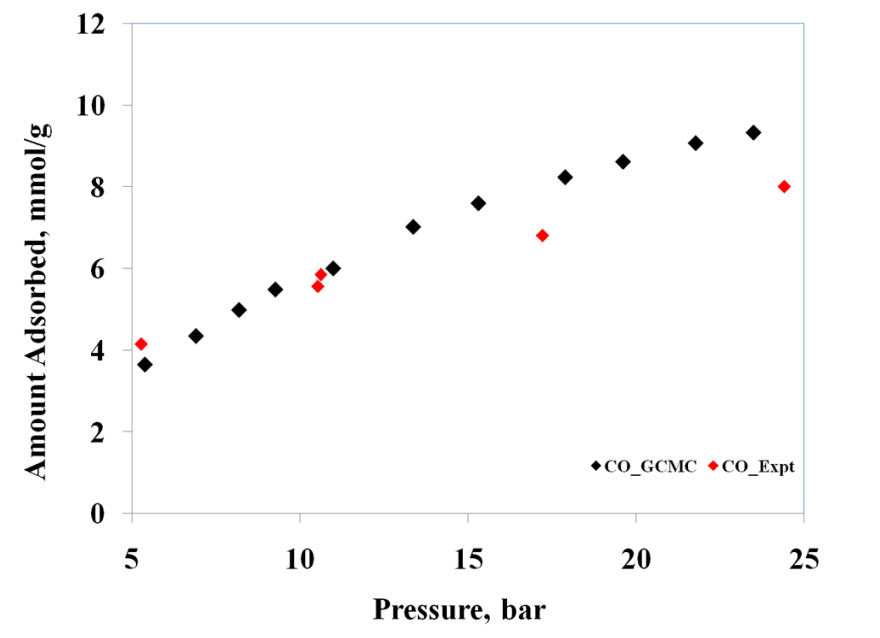

Figure 5.12: Comparison of GCMC simulation data [56] with experimental data [55] of CO adsorption on Cu-BTC at high pressure regime

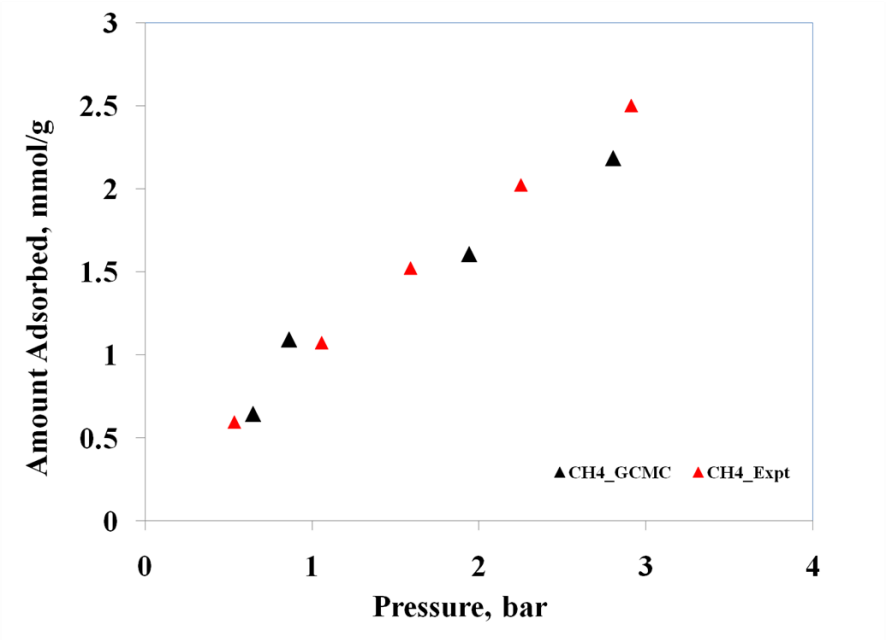

Figure 5.13: Comparison of GCMC simulation data [56] with experimental data [55] of CH_4 adsorption on Cu-BTC at low pressure regime

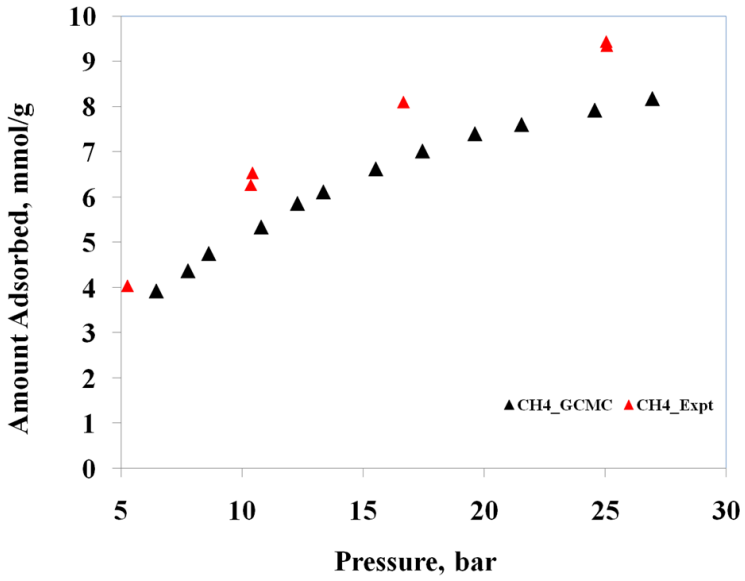

Figure 5.14: Comparison of GCMC simulation data [56] with experimental data [55] of CH_4 adsorption on Cu-BTC at high pressure regime

Table 5.10: Physical properties of some adsorbate molecules

Gas	Mol. wt. ($g\ mol^{-1}$)	liquid molar volume* ($cm^3\ mol^{-1}$)	kinetic dia. (Å)	Polarizability ($\times 10^{-25}\ cm^3$)	Dipole moment ($\times 10^{18}$ esu. cm)	Quadrupole moment ($\times 10^{-40}$ C. m^2)
CH_4	16	37.7	3.8	26.0	0.0	0.0
CO_2	44	33.3	3.3	26.3	0.0	14.3
CO	28	33.0	3.76	19.5	0.112	2.5

Figure 5.10 gives a direct comparison of adsorption of CO on Cu-BTC at similar conditions. Much can't be differentiated between GCMC simulation data and experimentally obtained data from the overall isotherm plot. But, if we divide the isotherm into a low pressure regime and an intermediate-high pressure regime then certain useful observations can be made.

It is a known fact that, in the low coverage region, the amount adsorbed is often correlated to the heat of adsorption. Thus, for CO, which is having a strong dipole (table 5.10), the effect and hence the difference is more pronounced and the simulation data under predicts the experimental data. The more favorable adsorption sites for CO intake would be metallic Cu sites.

In intermediate coverage, surface area dictates term whereas in high loading, the adsorption capacity is clearly limited to the pore volume. From figure 5.12 it is clear that simulation data over predicts the experimental data. The best reasoning to such an observation can be attributed to imperfections in MOF crystal matrix. Actually, GCMC simulation considers a perfect crystal without any discontinuity in structure and devoid of any impurities but in reality, crystal defect is a common phenomenon in material synthesis and there is always some solvated molecules occupying important spaces inside the porous network. Thus the actual pore volume and surface area calculated from experiments is less than that assumed in simulation study. Additionally, the effect is more pronounced for polar molecules as compared to non-polar molecules.

To have a comparison, similar exercise is carried out with CH_4 on Cu-BTC. As shown in the figures 5.13 and 5.14, the effects are less pronounced as compared to CO.

This difference in simulation and experimental data reflects on more rationality during comparison. Actually, crystal defects and presence of solvent molecules inside the adsorbent matrix during experimentation may lead to some anomalies in comparison with simulation results, since during simulation a perfect crystal is assumed.

5.3 Stability Study of Synthesized MOFs

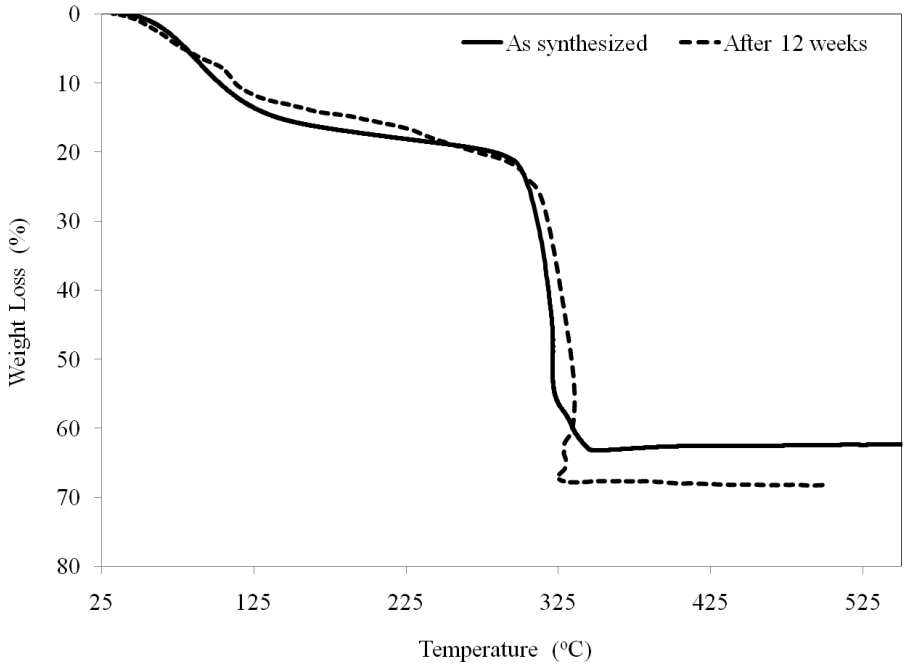

Figure 5.15: TGA analysis on Cu-BTC samples at two different conditions

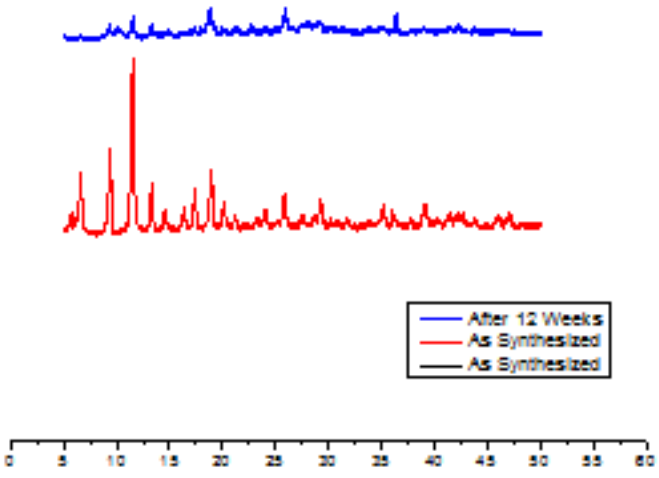

Figure 5.16: Powder XRD analysis on Cu-BTC samples at two different conditions

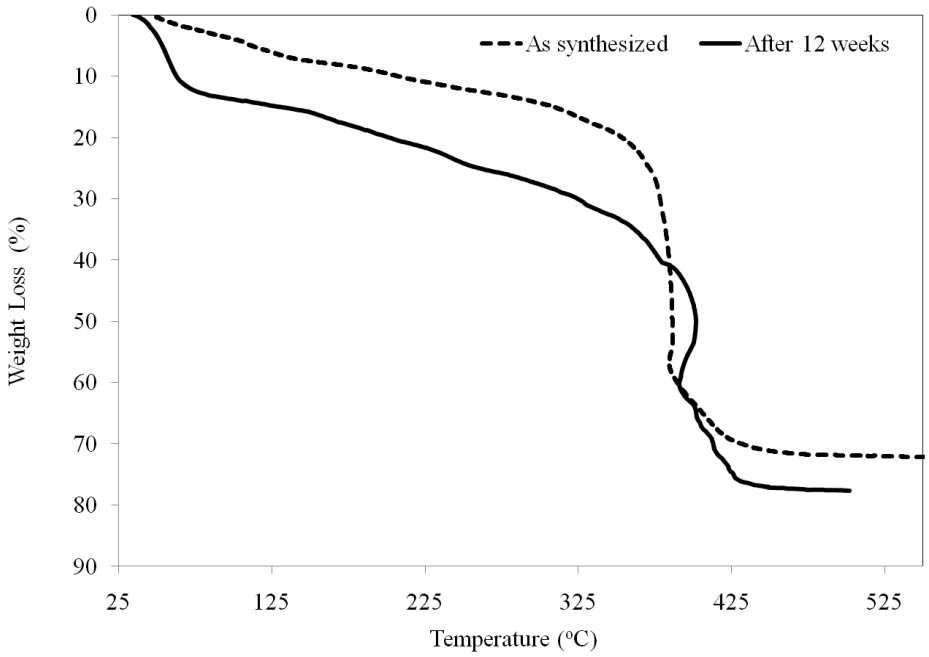

Figure 5.17: TGA analysis on Cr-BDC samples at two different conditions

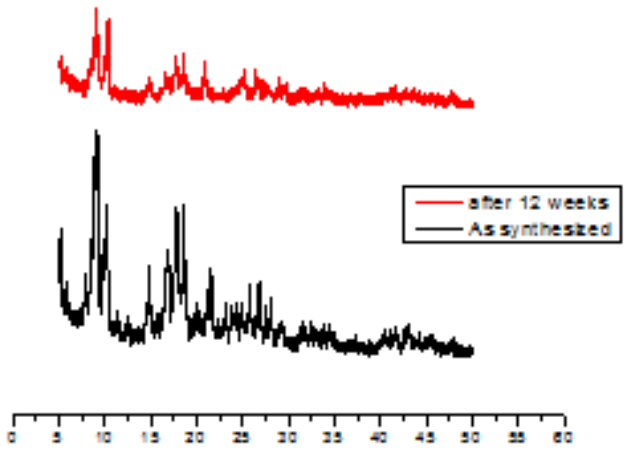

Figure 5.18: Powder XRD analysis on Cr-BDC samples at two different conditions

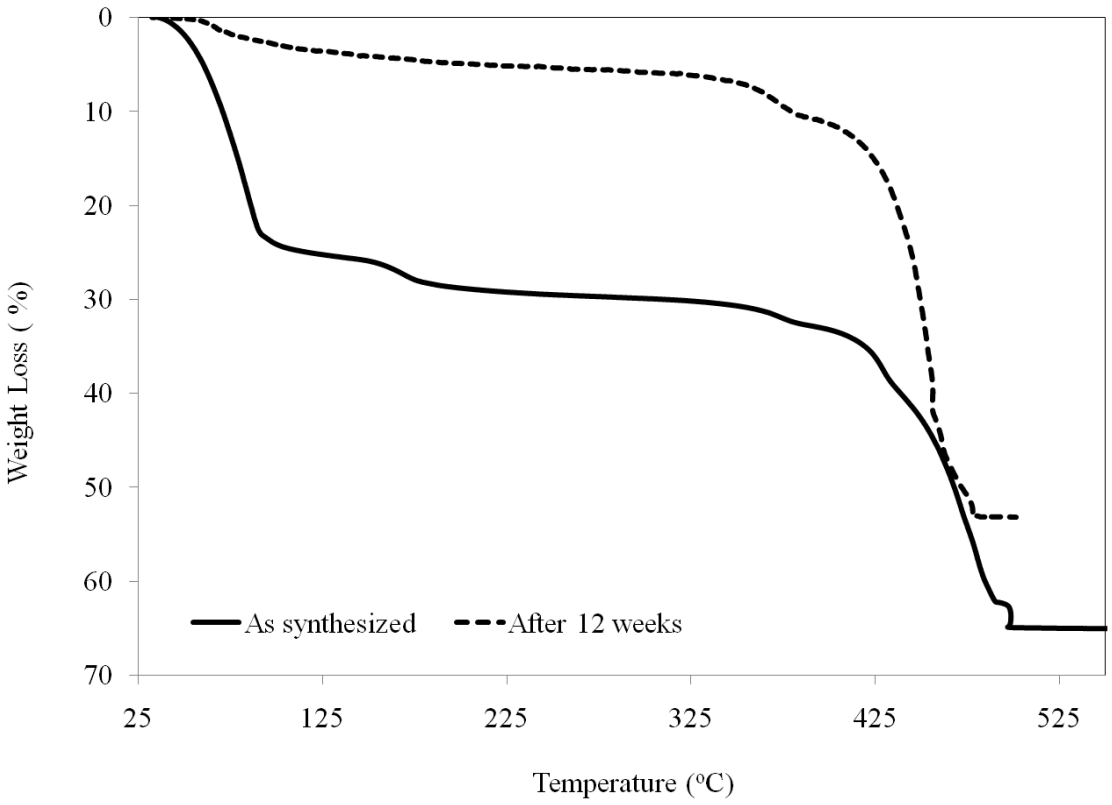

Figure 5.19: TGA analysis on Zn-BDC samples at two different conditions

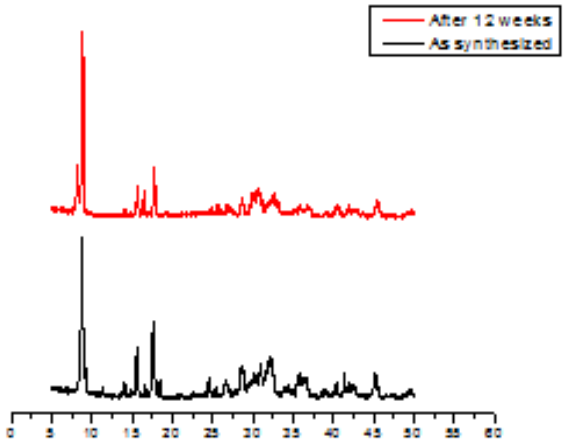

Figure 5.20: Powder XRD analysis of Zn-BDC samples at two different conditions

The success or failure of any adsorbent material depends on their endurance at different experimental conditions, especially at varying temperatures and under different solvent conditions. MOFs are known for their moderate thermal stability and lack of immunity under various organic/inorganic medium. In this work we continuously exposed synthesized MOF samples in a controlled fashion to atmosphere and studied the changes thereafter. Many interesting observations are made.

(I) Figure 5.15 and 5.16 shows the TGA and PXRD profiles for Cu-BTC before and after exposure to ambient conditions. The difference in the TGA profiles between as-synthesized sample and exposed sample are not as startling as it is expected to be. For either case the TGA profiles can be divided into 3 sections. The initial degradation between 25 to 125^{o}C is due to removal of moisture or traces of volatile matters. The fairly constant horizontal plateau between 125^{o}C to 275^{o}C is the stable zone and all experiments with Cu-BTC should be undertaken within this temperature regime. Beyond 275^{o}C, the Cu-BTC frameworks starts to collapse and the eventual end product is known to be CuO. The effect of controlled long exposure on Cu-BTC did not categorically reduce its framework integrity as is evident from the TGA. The only difference between the two graphs is due to higher percentage of moisture or trace amounts of methanol in as-synthesized sample and on prolonged controlled exposure it get reduced.

However, powder X-ray diffraction patterns for both the samples do show subtle differences. For example, in case of as-synthesized sample, sharp high intensity peaks confirms its crystallinity whereas for the second sample, the lack of intensity (although positioning of the major peaks remains intact) goes on to show the diminishing of crystallinity in the final product.

(II) TGA patterns of both Cr-BDC samples show exactly the same pattern. The only difference lies in the fact that the 12 weeks old sample appears to retain more moisture over the time of exposure and hence we have a larger weight loss profile. But, the ultimate stability of the sample does not get affected to a great deal. On comparison with Cu-BTC we can conclude Cr-BDC to be more hygroscopic. The presence of major peaks in the XRD profile also go into show that the structural integrity remained intact over the controlled long exposure. Overall thermal stability of Cr-BDC is found to be more than Cu-BTC.

(III) Thermally, Zn-BDC or MOF-5 is found to be the most stable out of the three MOFs that we have studied. Although TGA profiles of both the samples show a constant pattern, presence of a high percentage of DMF from post-synthesis treatment causes a greater weight-loss in the as-synthesized sample whereas over the prolonged exposure to atmosphere causes Zn-BDC to lose most of the solvated DMF and hence we can see a less weight loss for a 12 week old sample. However, the structural integrity of the crystals remains intact as is evident from the powder XRD profile.

To help corroborate our findings the SEM imaging of all the samples are taken.

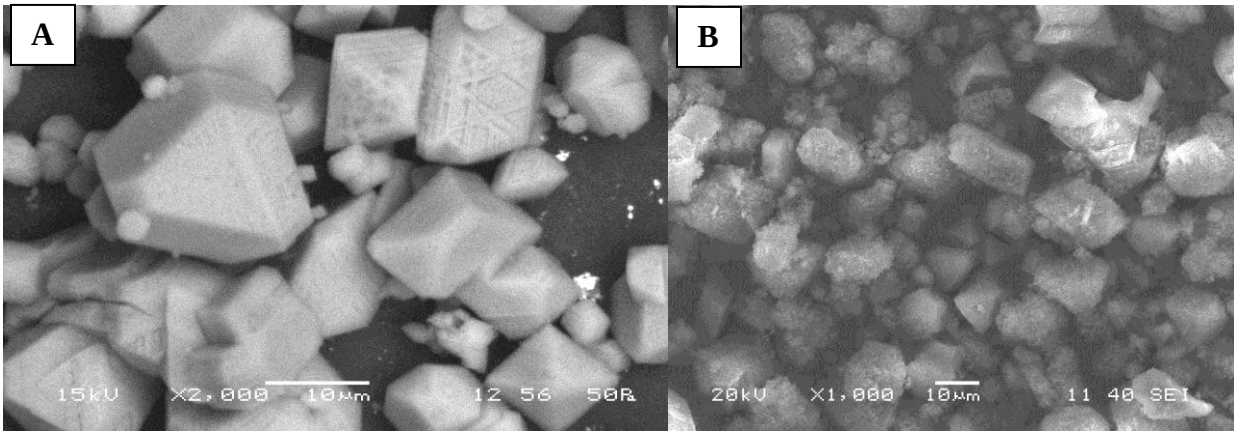

Figure 5.21: SEM images of Cu-BTC Samples (A) As-synthesized (B) Exposed sample

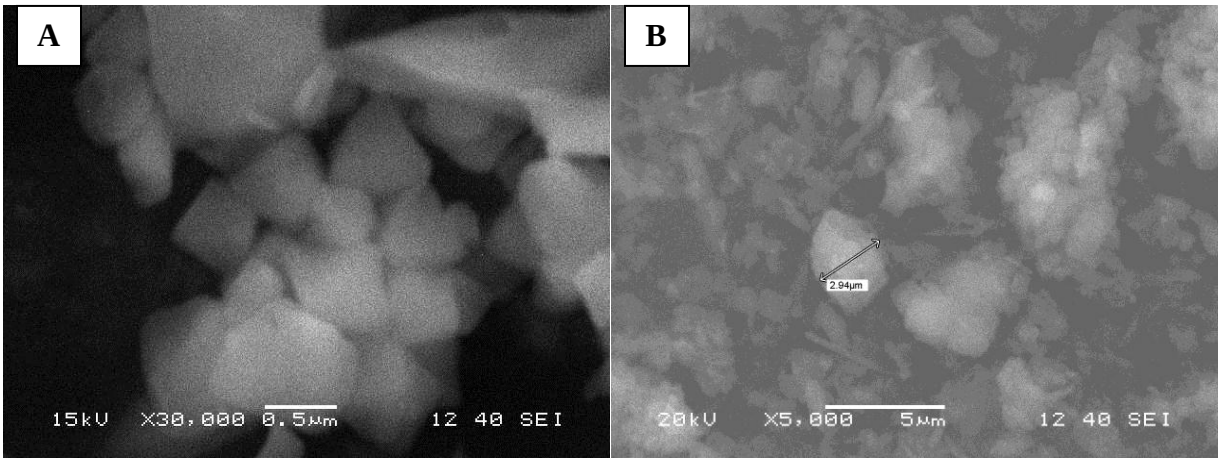

Figure 5.22: SEM images of Cr-BDC Samples (A) As-synthesized (B) Exposed sample

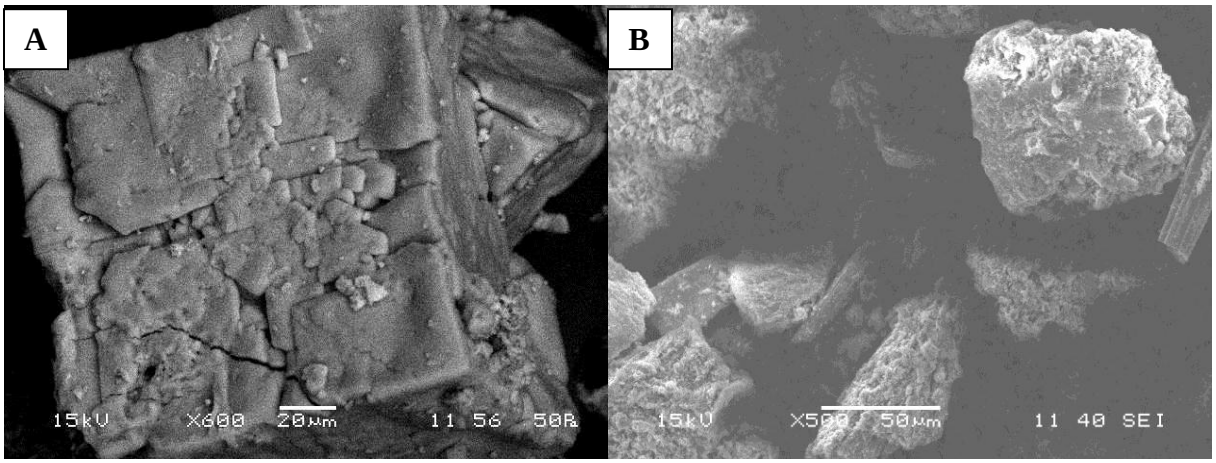

Figure 5.23: SEM images of Zn-BDC Samples (A) As-synthesized (B) Exposed sample

The scanning electron microscopy imaging too corroborates our findings. Although the surface morphology of all the MOF samples have changed considerably over the prolonged exposure to ambient conditions but the crystallinity remain intact. Thus, we could not observe any significant changes in TGA and PXRD.

CHAPTER 6

CONCLUSIONS AND FUTURE WORKS

In this work, we have highlighted the synthesis of 3 most versatile MOFs reported till date *viz*. Cu-BTC (or, HKUST-1), Cr-BDC (or, MIL-101) and Zn-BDC (or, MOF-5). Each of these MOFs after their successful synthesis and characterization were exposed to a regulated environmental condition to study the effect of moisture sensitivity. After detailed experimentation we concluded that a controlled exposure to ambient conditions didn't have a severe effect on MOF's thermal stability. Cr-BDC was found to be taking up more moisture during the course of time as compared to Cu-BTC and Zn-BDC. The degree of crystallinity appeared to be reduced over the time interval and surface morphology too gets affected.

A comprehensive literature review on adsorption of H_2, CO and CO_2 is carried out on these 3 MOFs. MOFs do show a superior adsorption capacity in comparison to any conventional adsorbents owing to their extraordinary surface area and pore volume. Various thermodynamic isotherm models are successfully fit with the experimental data (retrieved from literature). Interesting information on adsorbent characteristics and effect of polarities of the probe molecules on uptake capacity can be seen.

Our findings are summarized as:

(I) All the isotherm models are not equally efficient in predicting the adsorption behavior in low and high pressure regime. Freundlich-Langmuir model is seen to be the best in explaining the adsorption behavior irrespective of the type of probe or adsorbent surface.

(II) The experimental H_2 adsorption data as reported by various researchers varied considerably from lab to lab and H_2 adsorption on none of the adsorbents studied in this work satisfies the Department of Energy (DoE) target of 6.5 wt%.

(III) Cr-BDC (or, MIL-101) showed the highest affinity for CO_2. This uptake of CO_2 is the highest reported till date.

(IV) Although experimental data on CO adsorption on any MOF material is scarce, but still within our review, we have found Cr-BDC to have the highest loading of CO. The higher loading can be attributed to very high surface area (*ca*. 3000 m^2 g^{-1}) for Cr-BDC amongst the studied MOFs.

(V) The comparison of simulation with experimental data of CO and CH_4 on Cu-BTC has shown that for polar molecule e.g. CO, simulation data under predicts the experimental data whereas in the higher loading region simulation data over predicts. This is less marked for non-polar gas like CH_4. It is worth mentioning that even though there are variations in simulation result predictions with experimental data but still Grand Canonical Monte Carlo (GCMC) simulation is a strong method in predicting experimental excess adsorption data particularly when total pore volume information and single crystal XRD data is available.

Moreover, similar exercises can be done for other industrially important gases for a better understanding on adsorption. Elaborate GCMC simulation should be done assuming probable crystal imperfections for a better comparison. Newer derivatives of MOFs must be synthesized and studied with an aim on improved performances, before establishing itself to be a force to reckon with in near future.

REFERENCES

[1] http://en.wikipedia.org

[2] http://www.xamplified.com/adsorption/

[3] Yaghi, O. M., O'Keeffe, M., Ockwig, N. W., Chae, H. K., Eddaoudi, M., and Kim, J., "Reticular Synthesis and the design of New Materials," Nature, 423, 705-714 (2003).

[4] Rowsell, J. L. C., and Yaghi, O. M.," Metal–organic frameworks: a new class of porous materials," Micropor. Mesopor.Mater., 73, 3-14 (2004).

[5] Jinchen Liu, Jeffrey T. Culp, Sittichai Natesakhawat, Bradley C. Bockrath, Brian Zande, S. G. Sankar, Giovanni Garberoglio, and J. Karl Johnson, "Experimental and Theoretical Studies of Gas Adsorption in Cu3(BTC)2" J. Phys. Chem. C., 111, 9305-9313(2007).

[6] Chui, S. S.-Y., Lo, S. M.-F., Charmant, J. P. H., Orpen, A. G., and Williams, I. D.,"A Chemically Functionalizable Nanoporous material [Cu3(TMA)2(H2O)3]n," Science, 283, 1148-1150 (1999).

[7] Wang, Q.M., Shen, D., Bülow, M., Lau, M. L., Deng, S., Fitch, F. R., Lemcoff, N. O., Semanscin, J., "Metallo-organic molecular sieve for gas separation and purification," Micropor. Mesopor.Mater., 55, 217-230 (2002).

[8] Vishnyakov, A., Ravikovitch, P. I., Neimark, A. V., Bülow, M., Wang, Q. M.,"Nanopore structure and sorption properties of Cu-BTC metal-organic framework," Nano Lett., 3, 713-718 (2003).

[9] Schlichte, K., Kratzke, T., and Kaskel, S.,"Improved synthesis, thermal stability and catalytic properties of the metal-organic framework compound Cu3(BTC)2," Micropor. Mesopor.Mater., 73, 81-88 (2004).

[10] Millward, A. R., and Yaghi, O. M.," Metal-Organic Frameworks with Exceptionally High Capacity for Storage of Carbon Dioxide at Room Temperature," J. Am. Chem. Soc., 127, 17998-17999 (2005).

[11] Rowsell, J. L. C., and Yaghi, O. M., "Effects of Functionalization, Catenation, and Variation of the Metal Oxide and Organic Linking Units on the Low-Pressure Hydrogen Adsorption Properties of Metal-Organic Frameworks," J. Am. Chem. Soc., 128, 1304-1315 (2006).

[12] Krungleviciute, V., Lask, K., Heroux, L., Migone, A. D., Lee, J. -Y., Li, J., and Skoulidas, A.," Argon Adsorption on Cu3(Benzene-1,3,5-tricarboxylate)2(H2O)3 Metal-Organic Framework," Langmuir, 23, 3106-3109 (2007).

[13] Jiangfeng Yang, Qiang Zhao, Jinping Li , and Jinxiang Dong, " Synthesis of metal–organic framework MIL-101 in TMAOH-Cr(NO3)3-H2BDC-H2O and its hydrogen-storage behavior," Microporous and Mesoporous Materials, 130, 174–179 (2010).

[14] Do-Young Hong, Young Kyu Hwang, Christian Serre, Ge´rardFe´rey, and Jong-San Chang, "Porous Chromium Terephthalate MIL-101 with Coordinatively Unsaturated Sites: Surface Functionalization, Encapsulation, Sorption and Catalysis," Adv. Funct. Mater., 19, 1537–1552 (2009).

[15] Li, Y., and Yang, R.T., "Hydrogen Storage in Metal-Organic and Covalent-Organic Frameworks by Spillover," AIChE J., 54, 269-279 (2008).

[16] Senkovska, I. and Kaskel, S.," High pressure methane adsorption in the metal-organic frameworks Cu3(btc)2, Zn2(bdc)2dabco, and Cr3F(H2O)2O(bdc)3," Micropor. Mesopor.Mater., 112, 108-115 (2008).

[17] Li, H., Eddaoudi, M., O'Keeffe, M., and Yaghi O.M., "Design and synthesis of an exceptionally stable and highly porous metal–organic framework," Nature, 402, 276–279 (1999).

[18] Huang, L., Wang, H., Chen, J., Wang, Z., Sun, J., and Zhao, D., "Synthesis, morphology control, and properties of porous metal–organic coordination polymers," Micropor Mesopor Mater, 58(2), 105–114 (2003).

[19] Rowsell, J. L. C., Milward, A. R., Park, K. S., and Yaghi, O. M., "Hydrogen sorption in functionalized metal–organic frameworks," J. Am. Chem. Soc. 126(18), 5666–7 (2004).

[20] Panella, B., and Hirscher, M., "Hydrogen physisorption in metal– organic porous crystals," Adv. Mater. 17(5), 538–41 (2005).

[21] Panella, B., Hirscher, M., Putter, H., and Muller, U., "Hydrogen adsorption in metal–organic frameworks: Cu-MOFs and Zn-MOFs compared," AdvFunct Mater, 16(4), 520–4 (2006).

[22] Rowsell, J. L. C., Millward, A. R., Park, K. S., and Yaghi, O. M.," Hydrogen Sorption in Functionalized Metal-Organic Frameworks," J. Am. Chem. Soc., 126, 5666-5667 (2004).

[23] Wong-Foy, A. G., Matzger, A. J., and Yaghi, O. M., "Exceptional H_2 Saturation Uptake in Microporous Metal-Organic Frameworks," *J. Am. Chem. Soc.*, **128**, 3494-3495 (2006).

[24] Pan, L., Sander, M. B., Huang, X., Li, J., Smith, M., Bittner, E., Bockrath, B., and Karl Johnson, J.," Microporous Metal Organic Materials: Promising Candidates as Sorbents for Hydrogen Storage," *J. Am. Chem. Soc.*, **126**, 1308-1309 (2004).

[25] Férey, G., Latroche, M., Serre, C., Millange, F., Loiseau, T., and Percheron-Guégan, A., "Hydrogen adsorption in the nanoporous metal-benzenedicarboxylate$M(OH)(O_2C–C_6H_4–CO_2)$ ($M = Al^{3+}$, Cr^{3+}), MIL-53," *Chem. Commun.*, 2976-2977 (2003).

[26] Latroche, M., Surblé S., Serre, C., Mellot-Draznieks, C., Llewellyn, P. L., Lee, J. H, Chang, J. S., Jhung, S. H., and Férey, G., "Hydrogen Storage in the Giant-Pore Metal-Organic Frameworks MIL-100 and MIL-101," *Angew. Chem. Int. Ed.*, **45**, 8227-8231 (2006).

[27] Li, Y., and Yang, R. T.,"Significantly Enhanced Hydrogen Storage in Metal-Organic Frameworks via Spillover," *J. Am. Chem. Soc.*, **128**, 726-727 (2006).

[28] Van de Voorde, M., Verelst, H., and Baron, G.V., "Measurement of O_2-N_2 Binary Sorption on 5A Zeolite by Isotope Tracer and Perturbation Chromatography," *J. Porous Materials,* **2**, 51-57 (1995).

[29] Staudt, R., Herbst, A., Beutekamp S., and Harting, P., "Adsorption of Pure Gases and Mixtures on Porous Solids up to High Pressures," *Adsorption*, **11**, 379-384 (2005).

[30] Shen, D., and Bülow, M., "Comparison of Experimental Techniques for Measuring Isosteric Heat of Adsorption," *Adsorption*, **6**, 275-286 (2000).

[31] Talu, O., andZwiebel, I., "Multicomponent Adsorption Equilibria of Nonideal Mixtures", *AIChE J.*,**32,** 1263-1276 (1986).

[32] Li, Y., and Yang, R.T., "Gas Adsorption and storage in Metal-Organic Framework MOF-177," *Langmuir*, **23**, 12937-12944 (2007).

[33] Wang, S., Yang, Q., and Zhong, C.,"Adsorption and separation of binary mixtures in a metal-organic framework Cu-BTC: A computational study," *Sep. Purf. Tech.*, 6**0**, 30-35 (2008).

[34] Yazaydin, A.O., Snurr, R.Q., Park, T.-H., Koh, K., Liu, J., LeVan, M.D., Benin, A.I., Jakubczak, P., Lanuza, M., Galloway, D.B., Low, J.J., and Willis, R.R., "Screening of Metal-Organic Frameworks for Carbon Dioxide Capture from Flue Gas Using a Combined Experimental and Modeling Approach," *J. Am. Chem. Soc.*, **131**, 18198-18199 (2009).

[35] Myers, A.L., "Characterization of nanopores by standard enthalpy and entropy of adsorption of probe molecules," Colloids and Surfaces A, **241**, 9-14 (2004).

[36] Zhao, Z., Li, Z., and Lin, Y.S., "Adsorption and Diffusion of Carbon Dioxide on Metal-Organic Framework (MOF-5)," *Ind. Eng. Chem. Res.*, **48**, 10015-10020 (2009).

[37] Rosi, N. L., Eckert, J., Eddaoudi, M., Vodak, D. T., Kim, J., O'Keeffe, M., and Yaghi, O. M.," Hydrogen Storage in Microporous Metal-Organic Frameworks," *Science*, **300**, 1127-1129 (2003).

[38] Siperstein, F.R., and Myers, A.L., "Mixed-Gas Adsorption," *AIChE J.*, 47, 1141-1159 (2001).

[39] Dunne, J.A., Rao, M., Sircar, S., Gorte, R.J., and Myers, A.L.," Calorimetric Heats of Adsorption and Adsorption Isotherms. 2. O_2, N_2, Ar, CO_2, CH_4, C_2H_6, and SF_6 on NaX, H-ZSM-5, and Na-ZSM-5 Zeolites," *Langmuir*, **12**,5896-5904 (1996).

[40] García-Pérez, E., Gascón, J., Morales-Flórez, V., Castillo, J.M., Kapteijn, F., and Calero, S., "Identification of Adsorption sites in Cu-BTC by Experimentation and Molecular Simulation," *Langmuir*, 25, 1725-1731 (2009).

[41] Sun, M.S., Shah, D. B.,Xu, H. H., and Talu, O., "Adsorption Equilibria of C_1 to C_4 Alkanes, CO_2, and SF_6 on Silicalite," *J. Phys. Chem. B*,**102**, 1466-1473(1998).

[42] Golden, T.C., andSircar, S., "Gas Adsorption on Silicalite," *J. Coll. Inter. Sci.*, 162, 182-188 (1994).

[43] Dunne, J.A., Mariwala, R., Rao, M., Sircar, S., Gorte, R.J., and Myers A.L., "Calorimetric Heats of Adsorption and adsorption Isotherms.1. O_2, N_2, Ar, CO_2, CH_4, C_2H_6, and SF_6 on Silicalite," *Langmuir*, **12**, 5888-5895 (1996).

[44] Talu, O., Zhang, S.-Y., and Hayhurst, D.T., "Effect of Cations on Methane Adsorption by NaY, MgY, CaY, SrY, and BaY Zeolites," *J. Phys. Chem.*, **97**, 12894-12898 (1993).

[45] Li, P., and Tezel, F.H., "Pure and Binary Adsorption of Methane and Nitrogen by Silicalite," *J. Chem. Engg. Data*,**54**, 8-15 (2009).

[46] Liang, Z., Marshall, M., and Chaffee, A.L., "CO_2 Adsorption-Based Separation by Metal Organic framework (Cu-BTC) versus Zeolite (13X)," *Energy & Fuels*, **23**, 2785-2789 (2009).

[47] Gas Adsorption equilibria, experimental methods and Adsorptive Isotherms by jurgenU.Keller,Reinerstaudt

[48] http://en.wikipedia.org/wiki/Langmuir_adsorption_model

[49] NIST Chemistry web book [http://webbook.nist.gov/chemistry/]

[50] Chui, S. S.-Y., Lo, S. M.-F., Charmant, J. P. H., Orpen, A. G., and Williams, I. D.,"A Chemically Functionalizable Nanoporous material [Cu3(TMA)2(H2O)3]n," Science, 283, 1148-1150 (1999).

[51] Rowsell, J. L. C., and Yaghi, O. M., “Effects of Functionalization, Catenation, and Variation of the Metal Oxide and Organic Linking Units on the Low-Pressure Hydrogen Adsorption Properties of Metal-Organic Frameworks,” J. Am. Chem. Soc., 128, 1304-1315 (2006).

[52] Férey, G., Mellot-Draznieks, C., Serre, C., Millange, F., Dutour, J., Surblé S., and Margiolaki, I., “A Chromium Terephthalate-Based Solid with Unusually Large Pore Volumes and Surface Area,” Science, 309, 2040-2042 (2005).

[53] Henrik Fanø Clausen, Rasmus Damgaard Poulsen, Andrew D. Bond, Marie-Agnes S.Chevallier, Bo Brummerstedt Iversen, “Solvothermal synthesis of new metal organic framework structures in the zinc–terephthalic acid–dimethyl formamide system” Solid State Chemistry 178, 3342–3351(2005).

[54] Jinping Li, Shaojuan Cheng, Qiang Zhao, Peipei Long, Jinxiang Dong, “Synthesis and hydrogen-storage behavior of metal–organic framework MOF-5” hydrogen energy 34, 1377-1382 (2009).

[55] PradipChowdhury ,SamuelMekala, FriederDreisbach, Sasidhar Gumma a, “Adsorption of CO, CO2 and CH4 on Cu-BTC and MIL-101 metal organic frameworks: Effect of open metal sites and adsorbate polarity”, Microporous and Mesoporous Materials 152 (2012) 246–252

[56] Jagadeswara R. Karra, and Krista S. Walton, “Effect of Open Metal Sites on Adsorption of Polar and Nonpolar Molecules in Metal”, Langmuir, 2008, 24 (16), 8620-8626

[57] Karra, J. R.; Walton, K. S. "Molecular Simulations and Experimental Studies of CO 2 , CO , and N 2 Adsorption in Metal-Organic Frameworks". Adsorption Journal Of The International Adsorption Society 2010, 15735-15740

[58] Aprea, P.; Caputo, D.; Gargiulo, N.; Iucolano, F.; Pepe, F.; Ii, F.; Tecchio, P.; Ingegneria, D.; Roma, P. “Modeling Carbon Dioxide Adsorption on Microporous Substrates : Comparison between Cu-BTC Metal-Organic Framework and 13X Zeolitic Molecular Sieve”. Engineering 2010, 3655-3661.

[59] Saha, D.; Bao, Z. on “MOF-5 , MOF-177 , and Zeolite 5A”. Environmental Science & Technology 2010, 44, 1820-1826.

APPENDIX

Table A.I: H_2 adsorption isotherm data on Cu-BTC [23] samples at 77 K

Pressure (KPa)	**Amount Adsorbed (mmol g^{-1})**
91.80	7.68
158.44	9.42
246.91	11.01
444.46	11.88
839.26	13.04
1168.00	13.62
1606.30	14.20
2088.10	14.35
2570.20	14.93
3030.10	14.93
3599.60	15.22
4344.30	15.51
5461.00	15.51
6621.70	15.65
7738.80	16.23
8789.70	15.94

Table A.II: H_2 adsorption isotherm data on Cr-BDC [15] samples at 77 K

Pressure (KPa)	Amount Adsorbed (mmol g^{-1})
1.09	0.40
6.26	2.02
10.35	2.83
15.55	3.69
25.66	4.92
36.06	5.91
46.19	6.69
55.49	7.44
65.90	7.98
75.76	8.56
86.44	9.14
95.75	9.52

Table A.III: H_2 adsorption isotherm data on Zn-BDC [21] samples at 87 K

Pressure (KPa)	Amount Adsorbed (mmol g^{-1})
281.06	5.55
300.27	6.49
340.63	7.16
442.31	8.37
441.77	8.71
543.45	9.93
686.25	11.36
746.91	12.32
828.29	13.28
1074.20	15.08
1918.30	18.72
4235.50	21.31
4794.40	21.81

Table A.IV: CO_2 adsorption isotherm data on Cu-BTC [58] samples at 293 K

Pressure (KPa)	**Amount Adsorbed (mmol g^{-1})**
1.60	0.05
6.78	0.43
14.36	0.91
26.71	1.73
53.83	3.36
94.94	5.28
101.72	5.60

Table A.V: CO_2 adsorption isotherm data on Cr-BDC [55] samples at 318 K

Pressure (KPa)	**Amount Adsorbed (mmol g^{-1})**
1	0.12
2	0.2
6	0.42
13	0.69
29	1.09
54	1.62
101	2.38
168	3.29
269	4.43
398	5.68
531	6.82
721	8.35
936	9.74
1329	12.06
1857	14.77
2625	18.13
3429	20.63
4526	21.3

Table A.VI: CO_2 adsorption isotherm data on Zn-BDC [59] samples at 298 K

Pressure (KPa)	**Amount Adsorbed (mmol g^{-1})**
1.69	0.04
3.38	0.04
5.36	0.08
11.00	0.11
18.33	0.22
22.55	0.31
31.58	0.34
35.25	0.39
43.42	0.47
47.66	0.46
56.96	0.54
59.78	0.57
68.25	0.62
71.35	0.65
73.61	0.65
81.79	0.71
85.45	0.72
95.04	0.74
98.15	0.74
102.10	0.74
104.36	0.74
106.05	0.74

Table A.VII: CO adsorption isotherm data on Cu-BTC [56] samples at 295K

Pressure (KPa)	Amount Adsorbed (mmol g^{-1})
9.1783	0.0682
14.5100	0.1369
22.1280	0.2330
32.4610	0.3011
42.0130	0.3831
53.9160	0.4092
67.2830	0.5323
84.1330	0.6272
99.8400	0.7084

Table A.VIII: CO adsorption isotherm data on Cr-BDC [55] samples at 318 K

Pressure (KPa)	Amount Adsorbed (mmol g^{-1})
5.00	0.16
12.00	0.26
53.00	0.48
106.00	0.61
159.00	0.72
227.00	0.81
293.00	0.94
533.00	1.26
1,070.00	1.87
1,735.00	2.49
2,626.00	3.19
3,552.00	3.90
5,002.00	4.60
6,453.00	5.16

Table A.IX: CO adsorption isotherm data on Zn-BDC [57] samples at 298 K

Pressure (KPa)	**Amount Adsorbed (mmol g^{-1})**
4.31	0.03
9.69	0.07
19.92	0.14
29.62	0.21
40.39	0.28
49.54	0.36
59.77	0.43
69.46	0.49
78.08	0.57
90.46	0.64
120.08	0.84

RESEARCH PUBLICATIONS

[1] Vinay Agarwal, K Bantraj, and Pradip Chowdhury, "Stability analysis and a systematic review on study of gas adsorption of CO_2, CH_4 and CO on Cu-BTC and Cr-BDC Metal Organic Frameworks," ***to be submitted***.